Enhancement of Extratropical Cyclogenesis by a Mesoscale Convective System

DA-LIN ZHANG AND RICHARD HARVEY

Department of Atmospheric and Oceanic Sciences, McGill University, Montreal, Quebec, Canada

(Manuscript received 11 January 1994, in final form 30 August 1994)

ABSTRACT

Considerable progress has been made in the past decades on understanding the life cycle of rapidly deepening winter cyclones. However, little attention has been paid to the role that mesoscale convective systems (MCSs) play during extratropical cyclogenesis within weak baroclinic environments. In this study, the impact of an MCS on the subsequent surface cyclogenesis is investigated by extending the previously documented 21-h simulation of the 10–11 June 1985 PRE-STORM squall line to 36 hours. The model reproduces the meteorological events from the initiation to the dissipation of the squall system and then to the formation of a surface cyclone and the amplification of midlevel baroclinic waves, as verified against all available observations.

It is found that the squall line is initiated ahead of a weak surface cold front with the aid of baroclinic forcing. Once initiated, however, the prefrontal squall system is primarily driven by the interaction of convectively generated circulations with a conditionally unstable environment. As it rapidly intensifies and accelerates eastward, the squall system amplifies a midlevel short wave by warming the upper troposphere and cooling the lower troposphere, and then forces it to move with the system. On the other hand, the movement of a low to midlevel thermal wave is primarily determined by adiabatic processes. Thus, the convective system tends to enhance the larger-scale baroclinicity and increase the phase lag between the pressure and thermal waves such that the baroclinic environment becomes more favorable for the subsequent surface cyclogenesis.

The role of moist convection in the surface cyclogenesis is examined by comparing simulations with and without the convective system. It is found that, in the absence of moist convection, the model also produces a surface cyclone, but with much weaker intensity, much smaller horizontal extent, and much slower displacement. The relationships of convectively generated mesovortices and wake lows to the surface cyclogenesis are also examined.

1. Introduction

The effects of moist convection on extratropical cyclogenesis have been extensively studied for many years (see the recent reviews by Reed 1990; Hoskins 1990; Uccellini 1990; Anthes 1990). The earliest studies can be traced back to the nineteenth century when the first mechanism proposed to explain midlatitude cyclogenesis was latent heat released from precipitation near the center of storms. Prevailing thought then shifted from this essentially thermal origin of cyclones to a more dynamical argument, for example, the pioneering work of Margules (1903) on the dry energetics of storms, the creation of the famous Bergen School of cyclones in the 1920s, and the breakthrough of baroclinic theory by Charney (1947) and Eady (1949). According to the theory strong temperature gradients, low static stability, and a phase lag between the mass and wind fields are the basic ingredients for amplifying baroclinic disturbances.

Interest in latent heating effects was revived in the 1950s with the introduction of numerical weather prediction models. Early numerical studies, such as Aubert (1957) and Danard (1964, 1966), used quasigeostrophic models to examine the importance of latent heating on cyclone-scale motions. These studies demonstrated that latent heat release from precipitation (then only on the grid scale) tends to increase the upper-level and decrease the lower-level height of isobaric surfaces, thereby leading to the deepening of cyclones and acceleration of their movement. The deepening of cyclones was shown to be achieved through production of additional available potential energy (APE) and an increased rate of conversion from potential to kinetic energy. Growing attention was paid to the effects of cumulus convection on extratropical cyclogenesis after Riehl and Malkus (1961), Charney and Eliassen (1964), and Kuo (1965) established the importance of cumulus convection in the development of tropical disturbances. For example, Tracton (1973) and Bosart (1981) argued that cumulus convection in the vicinity of the cyclone center could play a crucial part in the rapid intensification and even in the initiation of cyclones. Gyakum (1983) showed evidence to suggest that the extreme development of the *Queen Elizabeth II* cyclone was a result of the latent heat release

Corresponding author address: Dr. Da-Lin Zhang, Department of Atmospheric and Oceanic Sciences, McGill University, 805 Sherbrooke Street West, Montreal, Quebec H3A 2K6, Canada.
E-mail: dzhang@zephyr.meteo.mcgill.ca

in organized cumulus convection. Results of Tracton (1973) and Gyakum (1983) also exhibited greater deepening rates when a higher proportion of latent heating was released in the lower troposphere. These results have significant implications with respect to the relative importance of convective versus stratiform precipitation in surface cyclogenesis. This is because stratiform precipitation associated with cyclonic storms tends to produce a heating maximum at a relatively lower level than cumulus convection,[1] thus being more favorable for cyclogenesis. This result was confirmed by numerical simulations conducted by Anthes and Keyser (1979), Kuo and Reed (1988), and others in which both cumulus parameterization and grid-scale condensation schemes were implemented.

A number of more recent studies have stressed that the impact of diabatic heating on cyclogenesis, whether it be stratiform or convective in nature, should be viewed as a nonlinear problem rather than a simple linear addition to dry dynamics (e.g., Smith et al. 1984; Uccellini et al. 1987; Pauley and Smith 1988; Kuo et al. 1991). Attempts at gaining more physical insight into this nonlinearity have also been made from an isentropic potential vorticity (IPV) perspective (Hoskins et al. 1985; Davis and Emanuel 1991) to isolate the effects of nonconservative processes on dry dynamics. Latent heating in the ascending flow tends to increase the magnitude of IPV below and decrease it above, thereby enhancing the low-level cyclonic circulation. However, a recent study by Davis et al. (1993) showed that such a superposition of positive IPV onto the dry dynamics does not alter the basic development mechanism of cyclones. In other words, these systems are baroclinically driven in nature and they are only modulated by diabatic heating.

Despite the considerable research effort devoted to extratropical cyclogenesis, the majority of previous studies have only focused on rapidly deepening storms that occurred during the cold season or over ocean surfaces (Sanders and Gyakum 1980). Much less attention has been paid to extratropical cyclogenesis that occurred within weak baroclinic environments. On the other hand, a growing number of studies on mesocyclones, which occurred during the warm season, have appeared in the recent literature (e.g., Houze 1977; Zhang and Fritsch 1987, 1988b; Brandes 1990; Bartels and Maddox 1991; Biggerstaff and Houze 1991b; Johnson and Bartels 1992; Zhang 1992; Fritsch et al. 1994). In contrast to the baroclinic systems reviewed above, these mesocyclones, ranging from 50 to 500 km in scale, are convectively driven in nature and mostly associated with organized mesoscale convective systems (MCSs). Zhang and Fritsch (1988a) and Zhang (1992) have provided extensive discussions on the processes leading to mesocyclogenesis. It could occur as a result of either the low- to midlevel latent heat release in mesoscale ascent (Bosart and Sanders 1981; Zhang and Fritsch 1988b; Menard and Fritsch 1989) or the mid- to upper-level diabatic cooling in mesoscale descent (Brandes 1990; Biggerstaff and Houze 1991b; Zhang 1992). For a warming-induced mesocyclone, a midlevel warm-core structure can be expected when latent heating exceeds upward adiabatic cooling, and the cyclonic circulation will be maintained through the thermal wind relationship. By comparison, a cooling-induced mesocyclone is characterized by diabatic cooling above and adiabatic warming below, so its genesis occurs through either tilting of horizontal vorticity or vortex stretching, depending upon the magnitude of mid- to upper-level wind shears. These results led Zhang (1992) to postulate that mesocyclogenesis may be one of the basic dynamic effects of MCSs on their larger-scale environments, since mesocyclones can be induced by either latent heating in mesoscale ascent or diabatic cooling in mesoscale descent.

The purpose of the present study is to investigate the roles of deep convection and its interaction with a baroclinic environment in extratropical surface cyclogenesis, using a 36-h high-resolution simulation of the 10–11 June 1985 prefrontal squall line that occurred during the Preliminary Regional Experiment for STORM-Central (PRE-STORM, see Cunning 1986). This work is an extension of the previously documented 21-h simulation of the same case by Zhang et al. (1989, hereafter ZGP) and Zhang and Gao (1989, hereafter ZG). Because of the development of many classic squall-line signatures, this PRE-STORM squall system has been the subject of numerous studies [e.g., Augustine and Zipser 1987; Smull and Houze 1987; Johnson and Hamilton 1988, hereafter JH; Rutledge et al. 1988; ZGP; Biggerstaff and Houze 1991a,b]. Of particular interest for the present study is that the surface cyclogenesis did not become evident until *after* the prefrontal squall system completely dissipated (see JH). Previous studies only showed examples in which surface cyclogenesis occurred in pace with more rapid latent heat release. Thus, the scenario in the present case raises several questions. For instance, was there any relationship between the squall line and its subsequent cyclogenesis? If so, why did the cyclogenesis not become evident until after the dissipation of the squall system? Since the squall system developed in a baroclinic environment (see JH and ZGP), how did it interact with the baroclinic forcing in the processes lead-

[1] It should be noted that the vertical heating profiles of stratiform precipitation in summertime MCSs, that are of the sort of the conceptual model by Houze et al. (1989), differ from that which occurred in wintertime cyclonic storms. Specifically, stratiform precipitation in convective storms tends to have a heating maximum at upper levels at a height slightly lower than that associated with cumulus convection. This is particularly true in the 10–11 June 1985 squall system; both the observational analysis and model simulation showed that the latent heating axis in the stratiform region of the MCS tilts rearward with a peak located near 400 hPa (e.g., see Fig. 8 in Gallus and Johnson 1991; Fig. 3 in Zhang et al. 1994).

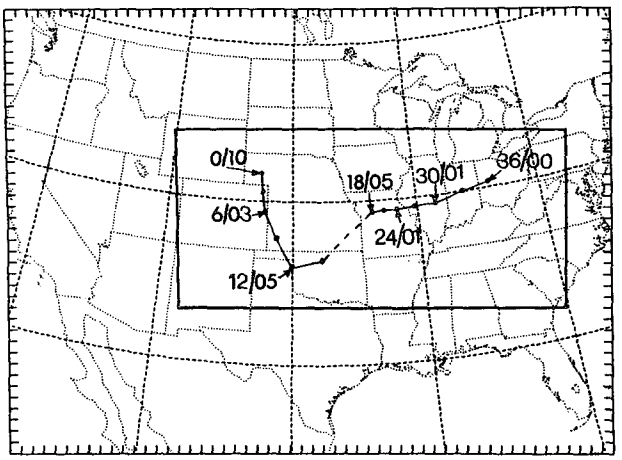

FIG. 1. The model nested-grid domain. Interior box indicates the fine-mesh portion of the domain. The intervals marked on the frame are mesh grids (75 km for coarse mesh). The 3-hourly positions of the simulated evolution from the mesolow to the surface cyclone are also given with the model hours and central pressures. Pressures are labeled in tens and unit hectopascals; similarly for the rest of figures.

ing to the cyclogenesis? Finally, to what extent did the convective and baroclinic forcings contribute to the genesis? Most of the previous studies have examined either baroclinically driven large-scale or convectively driven mesoscale cyclonic systems. Little work has been done on the roles of MCSs and their interaction with the large-scale baroclinicity in surface cyclogenesis.

The next section provides a description of the major model features and initial conditions used for the present study. Section 3 presents verification of the simulation against detailed observations and documents the events from the dissipation of the squall line to the mature stage of the cyclogenesis (see ZGP for detailed verification on the life cycle of the simulated squall line). The effects of the MCS on its larger-scale flow will also be examined. Section 4 discusses the individual roles of convective and baroclinic processes in the surface cyclogenesis, and shows the structure and evolution from a weak surface mesolow to a presquall low and finally to a surface cyclone. A summary and concluding remarks are given in the final section.

2. Model description and initial conditions

The model used for the present study is an improved version of The Pennsylvania State University/National Center for Atmospheric Research (PSU/NCAR) three-dimensional, hydrostatic, mesoscale model (Anthes et al. 1987), which is identical to that used by ZGP and ZG for the 21-h simulation of the same case. The major features of the model include (i) a two-way interactive nested-grid procedure (Zhang et al. 1986), (ii) an improved convective scheme of Fritsch and Chappell (1980) for the fine-mesh and Anthes et al. (1987) for the coarse-mesh portion of the nested-grid model, (iii) an explicit moisture scheme containing prognostic equations of cloud water (ice) and rainwater (snow) (Hsie et al. 1984; Zhang 1989; Dudhia 1989), and (iv) the Blackadar medium-resolution boundary-layer parameterization scheme (Zhang and Anthes 1982).

The nested-grid ratio is 1:3 with a fine-mesh length of 25 km and a coarse-mesh length of 75 km. The (x, y, σ) dimensions of the coarse and fine meshes are 55 $\times$ 41 $\times$ 19 and 106 $\times$ 49 $\times$ 19, respectively. The vertical terrain-following coordinate, σ, is defined as $\sigma = (p - p_t)/(p_s - p_t)$, where p_t is the pressure at the model top (in this case 70 hPa) and p_s is the surface pressure. Figure 1 shows the nested-grid configuration used for this study. A large fine-mesh domain is used, as compared to that used by ZGP and ZG, in order to include important disturbances that occurred at both the model initial and ending times (e.g., the cyclogenesis over Ohio Valley).

The nested-grid model is initialized at 1200 UTC 10 June 1985 with conventional meteorological observations using the same procedures as those described by ZGP. (No supplementary data were used for the model initialization, since the PRE-STORM network did not collect detailed observations until 2100 UTC 10 June when the squall line was initiated.) Figures 2 and 3 show the model initial conditions at 600 hPa and the surface, respectively. One can see that the large-scale conditions at 600 hPa were characterized by a baroclinic zone with weak cold advection to the west-northwest of the PRE-STORM network, and a midlevel shortwave trough over western Wyoming and Colorado (Fig. 2). The cold advection behind the trough axis was more significant at 700 hPa (see Fig. 3 in ZGP). At

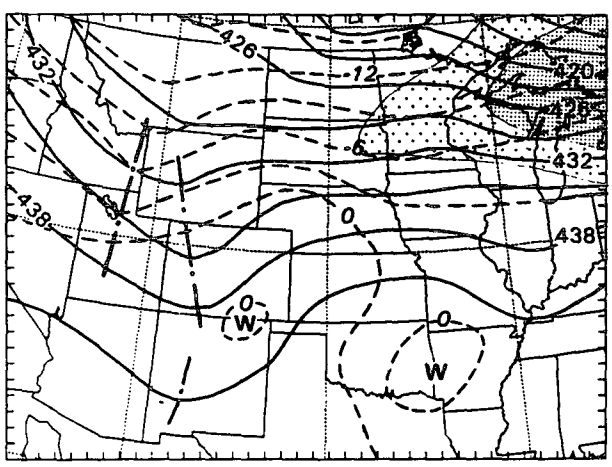

FIG. 2. Observed distribution of 600-hPa height (solid lines) at intervals of 3 dam and temperature (dashed lines) at intervals of 3°C for 1200 UTC 10 June 1985. Low- and medium-resolution shadings are used to indicate the distribution of wind speeds larger than 20 and 25 m s^{-1}, respectively. The chained lines indicate the axes of midlevel baroclinic troughs. The letters, "W" and "C," denote warm and cold centers.

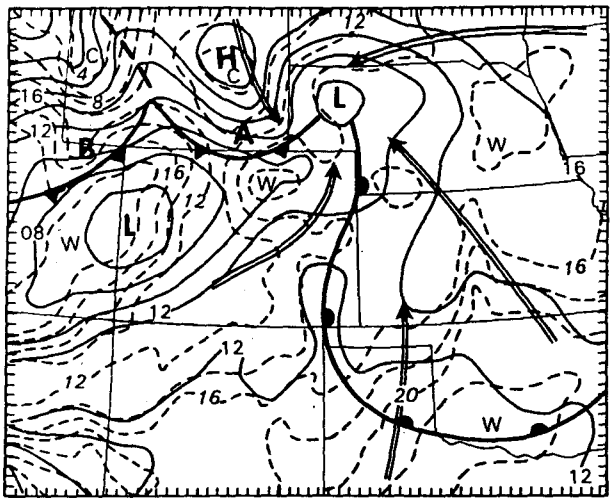

FIG. 3. Surface analysis of sea level pressure (solid lines) at intervals of 2 hPa and surface temperature (dashed lines) at intervals of 2°C for 1200 UTC 10 June 1985. Arrows indicate the selected streamlines in the surface layer (see ZGP). The intervals marked on the frame are mesh grids (25 km for fine mesh).

the surface (Fig. 3), a weak cold front was located over northern Colorado with two low pressure zones ahead: one over western Colorado and another over western Nebraska. The low-level flow was dominated by large-scale cyclonic circulation centered at the mesolow over western Nebraska. A quasi-stationary warm front extended from eastern Colorado to southern Oklahoma with a southwesterly to southerly low-level flow advecting high-θ_e air into the network area. (This warm front had been significantly modified by an earlier MCS that developed over the network, see Fig. 6 in ZGP.) A sounding taken over western Kansas exhibits a nearly saturated air mass below 700 hPa with considerable convective APE (see Fig. 5 in ZGP).

3. Case description and model verification

In this section, we verify the 36-h simulation against available observations (e.g., upper-air and surface analyses, satellite and radar imagery) and document the sequence of events from the model initial time to the surface cyclogenesis stage using both the observations and simulation. Since a number of previous studies have covered the life cycle of the squall system during the precyclogenesis phase from 1200 UTC 10 June to 0600 UTC 11 June (e.g., JH; Rutledge et al. 1988; ZGP; ZG), we describe it only briefly. We then present in detail the remaining 18 h, identify the events leading to the surface cyclogenesis, and finally examine the effects of moist convection on large-scale flow.

a. Pre-cyclogenesis stage

Both JH and ZGP showed that the squall line was initiated at 2100 UTC 10 June ahead of the surface cold front (i.e., segment "A" in Fig. 3) after it passed over the Rocky Mountains and interacted with the quasi-stationary warm front. The midlevel short wave appears to have also assisted the initiation of the prefrontal squall line. Then, the system intensified rapidly within a widespread convectively unstable environment over the network and propagated southeastward at a speed of 14–16 m s^{-1}. The daytime boundary layer development and the transport of high-θ_e air in the low-level southerly current provided such a favorable condition for rapid convective development (see JH and ZGP). During the intensifying stage, both the radar echoes and satellite imagery showed intense convective cells along the leading line and rapid expansion of stratiform cloudiness behind (Rutledge et al. 1988; Biggerstaff and Houze 1991a).

By 0300 UTC 11 June, the prefrontal squall line reached its peak intensity with the development of vigorous convective-scale and mesoscale circulations, such as an overturning updraft along the leading line, a front-to-rear (FTR) ascending flow associated with the generation of trailing stratiform precipitation, and a rear-to-front (RTF) descending flow (see JH; Rutledge et al. 1988; ZGP; ZG). In addition, Biggerstaff and Houze (1991b) and Zhang (1992) showed the development of a midlevel mesovortex in the trailing stratiform region of the squall system. At the surface, the system exhibits the typical pressure perturbations

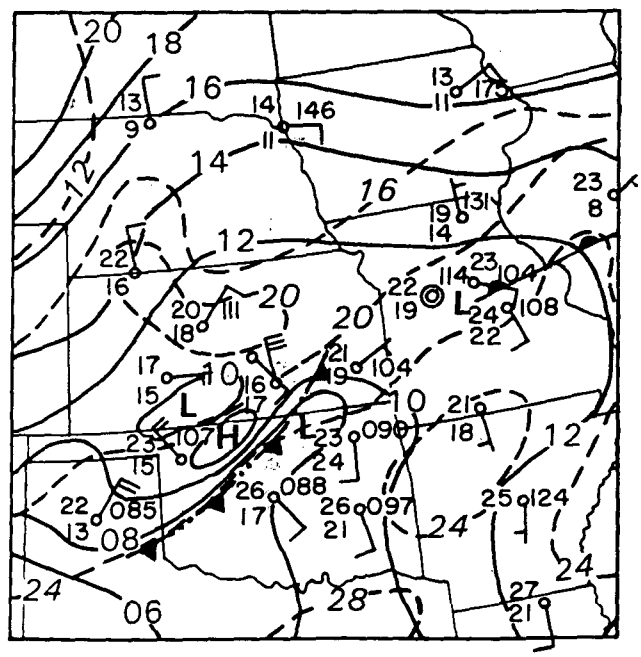

FIG. 4. Mesoanalysis of sea level pressure (solid lines) at intervals of 2 hPa and surface temperature (dashed lines) at intervals of 4°C for 0300 UTC 11 June 1985. Cold frontal symbols alternated with double dots indicate cold outflow boundaries or gust front. A full wind barb is 5 m s^{-1}. Only selected observations are plotted with meteorological convention.

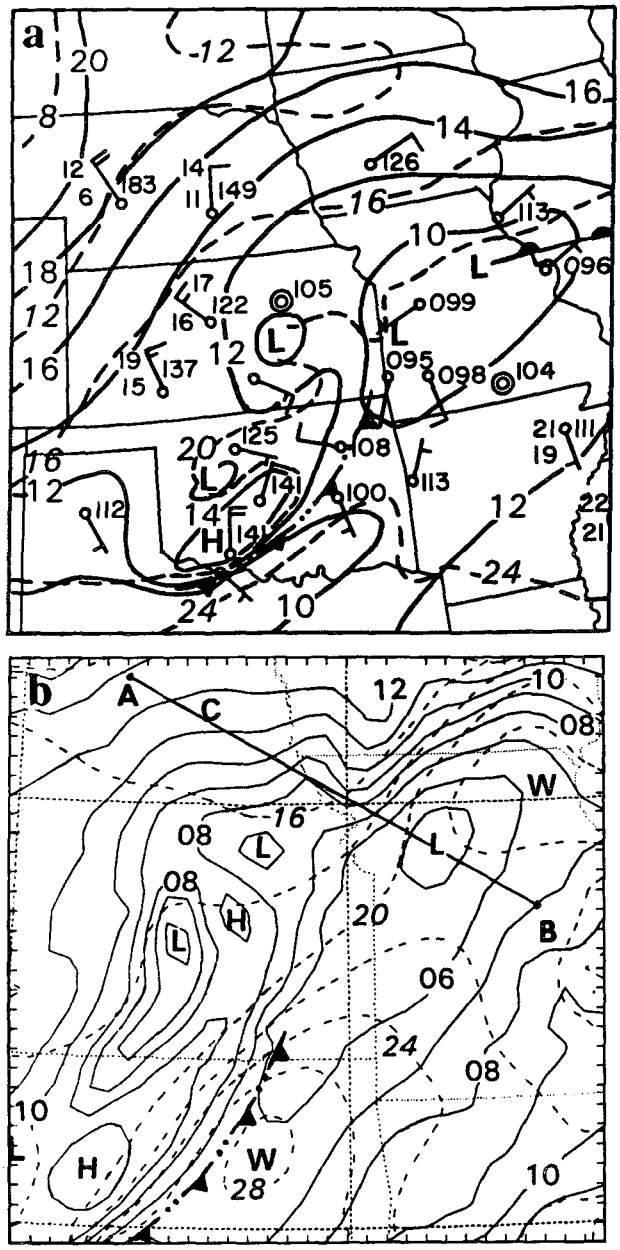

FIG. 5. (a) As in Fig. 4 but for 0600 UTC 11 June 1985; (b) sea level pressure (solid lines) at intervals of 1 hPa and surface temperature (dashed lines) at intervals of 2°C from 18-h simulation. The line A–B denotes the position of the vertical cross section used in Fig. 19a. Letters "W" and "C," "H" and "L" denote the centers of warm and cold air, high and low pressures. The intervals marked on the frame are mesh grids (25 km for fine mesh).

of midlatitude squall lines, that is, an elongated presquall mesolow, a squall mesohigh, and a wake low (Fig. 4). ZGP have traced the evolution of the presquall mesolow back to the prefrontal mesolow initially located over western Nebraska (see Figs. 1 and 3). The squall-related mesohigh is generally produced by convective downdrafts and evaporation of stratiform precipitation in the descending rear inflow (Johnson 1976; Zipser 1977; Houze et al. 1989), whereas the wake low develops hydrostatically as a consequence of adiabatic warming by descending unsaturated air within the rear inflow (see JH and ZG). The intense convectively generated downdrafts (or gust front) also accounted for the rapid propagation of the squall system. Note that the use of a larger-subdomain analysis, as compared to that used by JH and ZGP, allows us to see how these convectively generated perturbations were related to their larger-scale environment; namely, they were actually embedded in a large-scale weak cyclonic circulation, with a surface trough as well as the weak warm front that extended northeastward to central Illinois (and eventually into the Ohio Valley). These circulation structures depart substantially from the surface pressure patterns at the model initial time (cf. Figs. 3 and 4), mainly as a consequence of the development of the squall system. Because of the presence of the significant convective forcing,[2] the central portion of the large-scale trough system was dominated by the squall-line circulations (see JH, ZGP, and ZG).

Both radar and satellite observations reveal that the squall line entered a stage of rapid decay after 0300 UTC (JH; Rutledge et al. 1988) when it advanced into a convectively less unstable environment to the east of the network (see ZGP). At 0600 UTC (Fig. 5a), the squall line was well into the dissipation stage; it was characterized by weak convective cells along the leading line and weak FTR ascending flow in the stratiform region (see ZGP and ZG). As a result, the presquall mesolow became less controlled by the convective forcing, and a closed surface low began to emerge to the northeast of the squall system where the convective forcing was likely the weakest. This stage roughly marks the onset of the surface cyclogenesis. In contrast, the descending rear inflow still maintained its intensity, because there was still a sizable amount of condensate available for evaporation (see ZG). Thus, the intensity of the mesohigh and wake low was sustained even during this decaying stage. Note that the wake low split into two segments: one over western Oklahoma and the other over eastern Kansas; they tended to move southeastward and northeastward thereafter, respectively.

We begin to verify the model simulation in a subdomain framework against the detailed observations starting from the 18-h simulation, valid at 0600 UTC. It is apparent from Figs. 5a,b that the model reproduces extremely well the presquall mesolow to the east, the convectively generated mesohigh, and the split of the

[2] The convective forcing implied herein represents the collective effects of parameterized convection and grid-scale condensation associated with the squall system. It should be pointed out that the squall system is the primary convective forcing, particularly during the first 30-h period (see Fig. 6 in ZGP and Fig. 7 herein), that affects the subsequent cyclogenesis.

wake low into two segments. The basic temperature distribution is also reasonably well simulated. The model simulates a significant amount of grid-scale precipitation lagging behind the convective region, with more distributed to the northeast of the squall system (Fig. 6). More importantly, the model simulates the development of the closed surface low to the northeast of the squall system, except that it is more compact compared to the observations. This discrepancy may be attributable to the lack of high-resolution surface observations over Missouri. These disturbances are also embedded in a large-scale surface trough system. It should be noted that the horizontal extent of this surface trough is much greater than that at the model initial time (cf. Figs. 3 and 5) and in a "dry" simulation wherein the influence of the squall system was omitted (see Fig. 18 in ZG). This increase of the horizontal extent represents clearly the feedback effects of the squall system to its larger-scale environment.

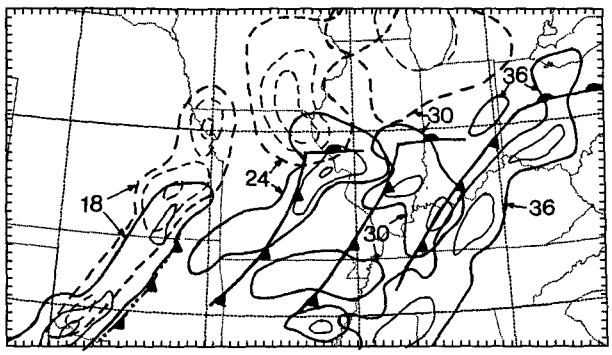

FIG. 6. The evolution of hourly convective (solid lines) and grid-scale (dashed lines) rainfall distribution in relation to the position of the surface cyclone from 18-h, 24-h, 30-h, and 36-h simulations. The rainfall rates are contoured at 1, 5, and 10 mm h^{-1}.

b. Cyclogenesis stage

By 0900 UTC, much of the squall system had propagated out of the PRE-STORM network. Radar reflectivities at 0800 UTC showed rapid weakening of convective cells along the leading line, followed by weak echoes from the two dissipating stratiform regions (see Rutledge et al. 1988 and satellite imagery in Fig. 7a). As a result, the convectively induced pressure perturbations were becoming much weaker and less distinct (see Fig. 8a). For instance, the southern wake low has been absorbed by the large-scale surface trough as it moved southeastward. The mesohigh has visibly shrunk in size and become more or less a mesoridge; it diminished shortly after the stratiform rainfall ceased. Meanwhile, the northern wake low has crossed the Kansas-Missouri border and merged with the major surface low located over eastern Missouri. Notably, this merging process coincided with somewhat greater organization of the background flow, as indicated by closed isobars of 1010 and 1012 hPa (cf. Figs. 5a and 8a). It also coincided with the deepening of the major surface low.

Very similar events also occur in the 21-h model simulation (see Fig. 8b). In particular, the simulation shows more clearly how the merging process takes place. That is, as the convective forcing rapidly weakens, the wake low advances northeastward, in a gravity wave fashion, at a speed roughly twice as large as that of the major surface low. This process seems to assist the more rapid deepening of the surface low during this period, since some warmer air associated with the wake low is being displaced into the overlying layers of the major low. Its central pressure drops from 1005 hPa at 18 h (Fig. 5b) to 1003 hPa at 21 h (Fig. 8b) and 1001 hPa at 24 h (Fig. 9b). It should be mentioned, however, that the model appears to suffer loss of mass, which is more evident in the south hereafter. This has caused a systematic reduction of surface pressures, that is, about 4 hPa averaged over the subdomain or 3–5 hPa overdeepening of the mesolow. This problem can be attributed partly to the inflow of imperfect initial and boundary conditions over tropical oceans and partly to the neglect of certain physical processes (e.g., infrared radiation in the free atmosphere). Nevertheless, the simulated pressure gradients and basic circulation patterns, which are more related to the dynamics of the system, are in good agreement with the observed.

By 1200 UTC 11 June, the squall line activity had nearly ceased, and chaotic cloud fragments were passively advected by the large-scale flow (Fig. 7b). However, more significant spinup of the large-scale cyclonic circulation occurred as the mesoscale pressure disturbances finally merged into a single pressure center near the Missouri–Illinois border (see Fig. 9). Surface winds in the vicinity of the center, which were never more than 2–3 m s^{-1} before, increased to northeasterly at 7–8 m s^{-1} on its northern flank[3] in about 3 hours. It is remarkable that the "background" flow adjusted to the mass field changes and became a typical developing extratropical cyclone in such a short time period. Meanwhile, these strong winds advected more cold air southward to enhance a cold front along the trough axis. For example, note how the 16°C isotherm, which remained over southern Iowa earlier, rapidly moved into the northern part of Missouri at this time (cf. Figs. 8a and 9a). Less apparent, but still visible, is the weak warm advection that occurs in the warm sector, as stations in eastern Arkansas and Missouri reported 2°–3°C warming over the previous 3 hours. These simultaneous increases in the cold and warm advection are indicative of baroclinic energy conversion

[3] The increase in surface winds over this region does not seem to be related to the early morning boundary-layer development since it occurs beneath an extensive area of stratiform clouds (e.g., see Fig. 7b).

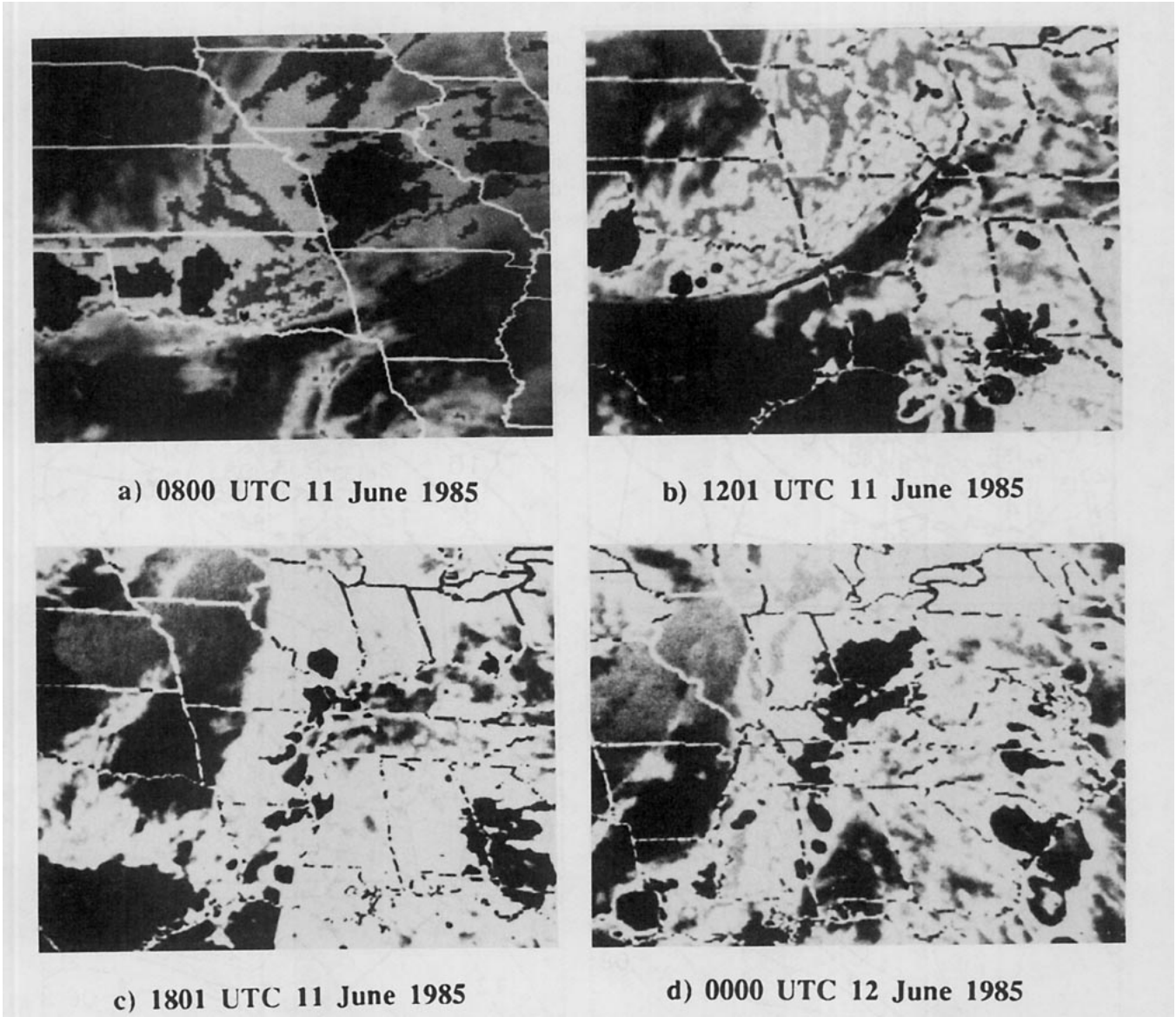

FIG. 7. Enhanced infrared satellite imagery between 0800 UTC 11 and 0000 UTC 12 June 1985.

for surface cyclogenesis. Note that this cyclonic spinup occurred after the nearly *complete* demise of the squall system. Two conclusions could be tentatively drawn from these results: (i) the squall system must have played an important but *indirect* role in the surface cyclogenesis, since it enhanced markedly the larger-scale pressure circulation during the squall period; and (ii) the large-scale baroclinicity, which had been obscured by the convective forcing earlier, came into play in the evolution of the surface cyclone. A thorough examination of these conclusions will be undertaken in the next section.

The model reproduces well the timing and the location of the final merging and subsequent surface cyclogenesis (Fig. 9b). The baroclinic development processes are more clearly apparent in the high-resolution simulation. For instance, strong cold advection occurs to the north and west of the cold front and weak warm advection occurs to the east—a typical structure for a "synoptic wave." This baroclinic development results in a packing of the isotherms just north and west of the low center, and more circular-shaped isobars near the center but still elongated structure on its larger scale. However, the model appears to have delayed somewhat the final dissipation of the squall-related convection. The convective activity at this time resembles that which occurred around 0800 UTC (cf. Figs. 6 and 7a,b); nevertheless, it becomes disorganized 2–3 h later. In contrast, the wide area of simulated grid-scale precipitation over Missouri and Iowa conforms reasonably well to the extensive (squall related) stratiform cloudiness to the north of the cyclone.

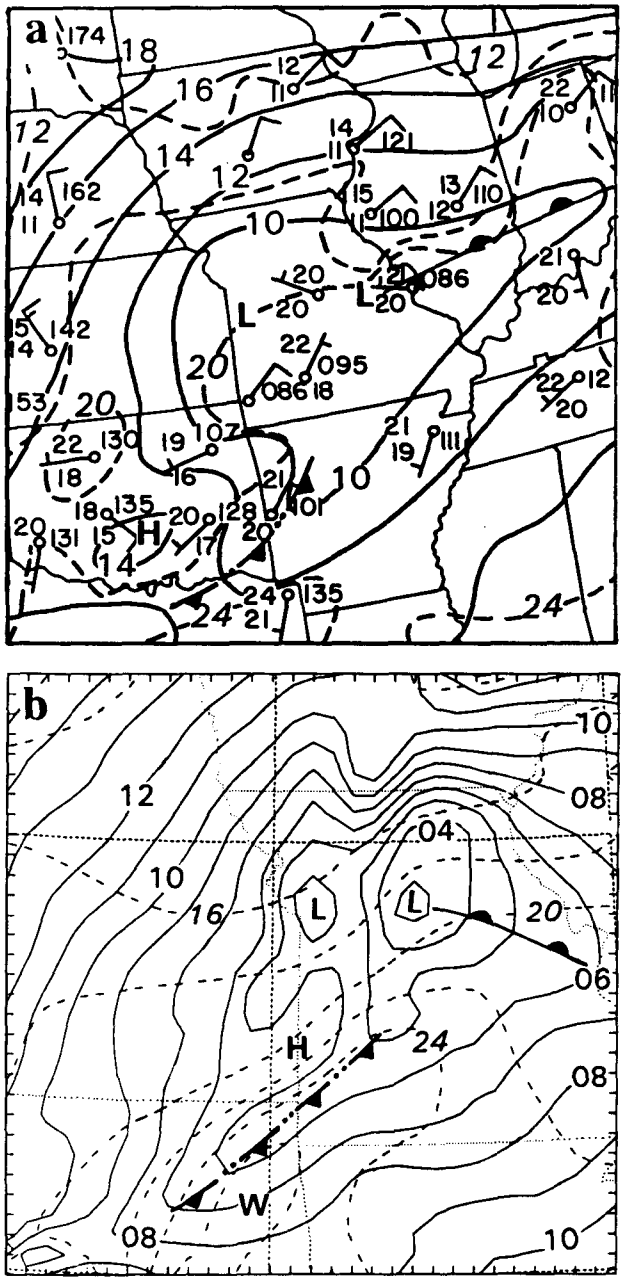

FIG. 8. As in Fig. 5 but for 0900 UTC 11 June 1985 and from 21-h simulation.

A particularly interesting way in which the squall line appears to modify the cyclonic system is by enhancing the cold frontogenesis (see Figs. 5, 8, and 9). Specifically, both observations and simulation show that as the gust front moves out of Oklahoma, the squall line leaves in its wake an extensive pool of cold air. This cold pool, although no longer forced by convective downdrafts, continues to propagate southeastward along with the surface trough. Thus, it acts to enhance and accelerate the original surface cold front, leading to sharper cross-frontal wind shifts along the pressure trough.

It is evident that the baroclinic processes would determine the subsequent evolution of the surface cyclone after the convective forcing diminished. Most notable during this stage was the rapid eastward acceleration and the intensification of the cyclone. By 1800 UTC 11 June, the cyclone had already crossed over to southwestern Indiana and deepened by a full 3 hPa to 1005

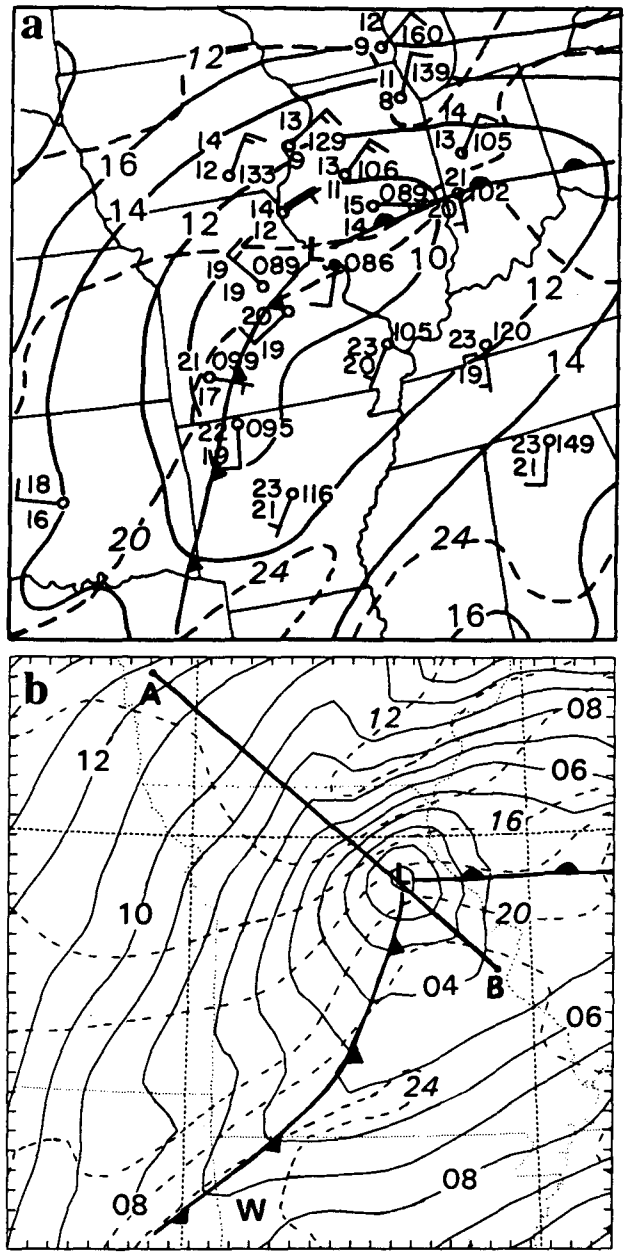

FIG. 9. As in Fig. 5 but for 1200 UTC 11 June 1985 and from 24-h simulation. The line A–B denotes the position of vertical cross section used in Fig. 19b.

hPa (Fig. 10a). Moreover, the cyclonic flow continued to intensify with wind reports of over 10 m s^{-1} in the northwestern quadrant and 5–8 m s^{-1} in the warm sector, further increasing the temperature gradients across the surface front. It should be noted that by this noon hour, the boundary layer had been significantly heated, particularly in the warm sector where surface temperatures had increased from 24° to 30°C during the previous 6 hours. Thus, a convective band with scattered cells was initiated along the cold front (Fig. 7c). This convective development did not appear to significantly affect the evolution of the surface cyclone. This is not surprising since the convective band was much less intense and less organized than the squall system that had just dissipated.

As compared to the observations, the simulated storm appears to move slightly slower and have a smaller deepening rate (cf. Figs. 10a,b). In spite of these minor differences, the rapid acceleration of the cyclone (see Fig. 1) and its related development are well captured. The position and intensity of the cold front, the stronger flow in the northwestern quadrant, and the general SW–NE orientation of the storm were reasonably handled. The boundary layer heating in the warm sector and the thermal structure behind the cold front are reproduced with reasonable accuracy. This boundary-layer development also caused scattered convective activity along the cold front, consistent with what appeared in the satellite imagery (cf. Figs. 6 and 7c). These results are very encouraging when considering that they were generated from initial conditions produced by conventional data. The results indicate that the model physical representations used for the present study are realistic enough to reproduce the life cycle of the squall system and its effects on the larger-scale environment.

At the end of our period of interest (i.e., 0000 UTC 12 June), both observations and simulation show further deepening of the cyclone with an intensified frontal zone, enhanced surface flow, and continued stronger cold advection behind the cold front (see Fig. 11). In particular, a 15 m s^{-1} wind was reported over Lake Erie about 200 km to the north of the cyclone. Both the simulation and observations also display the expansion of the convective band ahead of the cold front, with more cloudiness distributed near the center of the cyclone (see Fig. 7d). It is worth noting that the model simulates well the changes of convective rainfall from the "post gust frontal" type during the convectively driven stage (e.g., at 18 h) to the prefrontal type during the baroclinically driven stage (e.g., at 36 h), while the grid-scale precipitation center moves to the northeast of the cyclone under the southwesterly flow ahead of the short-wave trough (see Fig. 6). Finally, the National Meteorological Center (NMC) analysis indicates that the surface cyclone continued its deepening to 997 hPa and then occluded as it moved into the Atlantic Ocean 18 hours later (not shown).

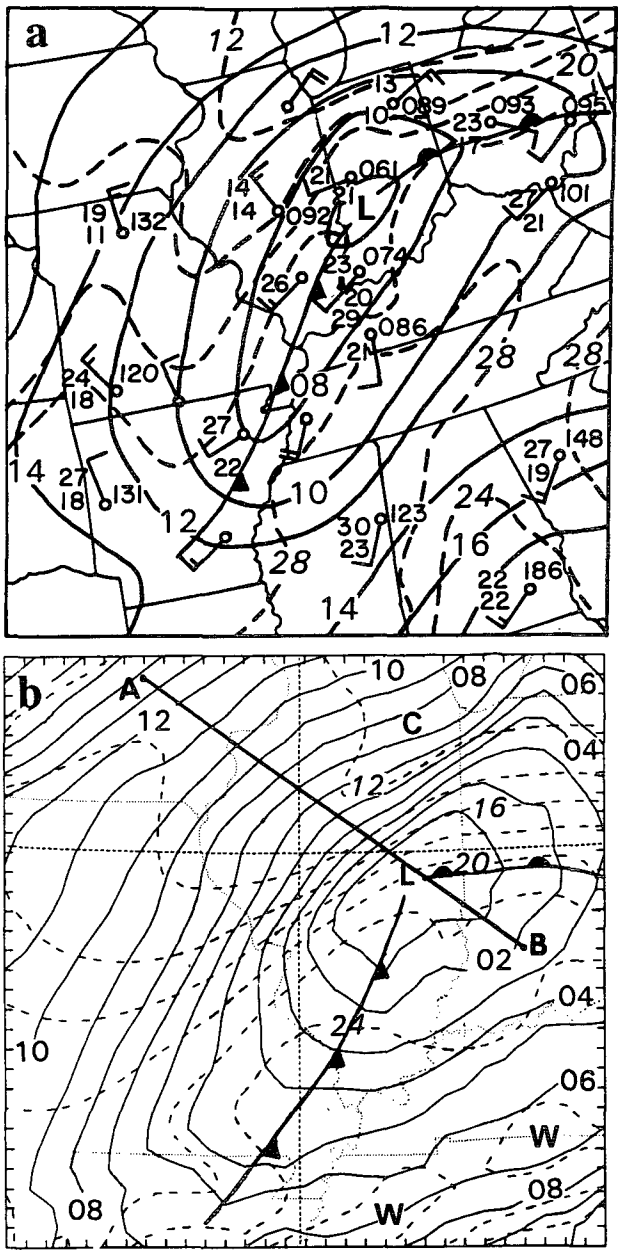

FIG. 10. As in Fig. 5 but for 1800 UTC 11 June 1985 and from 30-h simulation. The line A–B denotes the position of vertical cross section used in Fig. 19c.

c. *Evolution of the large-scale flow*

After showing an apparent effect of deep convection on the large-scale *surface* pressure circulations, it is necessary to also examine if the intense squall system produced any significant effect on the large-scale tropospheric flow. Thus, Fig. 12 shows the NMC analysis of the 600-hPa heights and temperatures at three synoptic times. At 0000 UTC 11 June, the squall line had been active for about 3 h and was located just ahead of

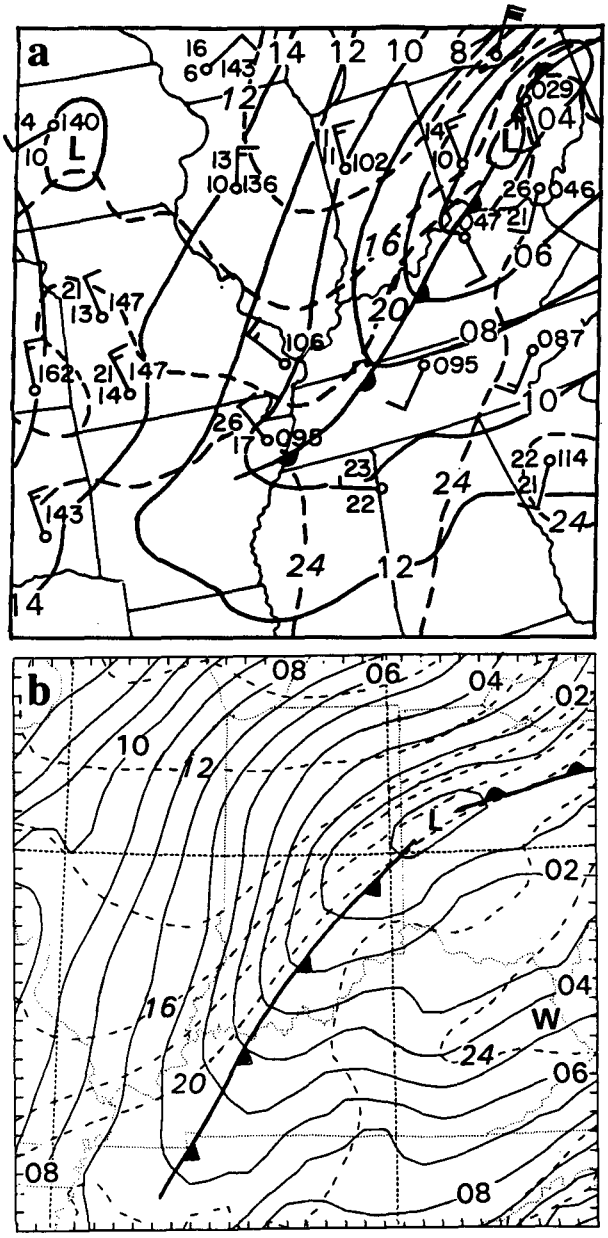

FIG. 11. As in Fig. 5 but for 0000 UTC 12 June 1985 and from 36-h simulation.

the 600-hPa pressure trough axis that was oriented from central Nebraska to the Oklahoma panhandle (cf. Fig. 6d in ZGP and Fig. 12a herein). Note that the thermal trough, after it passed the peak of the Rocky Mountains, displays a more favorable juxtaposition with the pressure wave than that at the initial time (cf. Figs. 2 and 12a); namely, the cold advection behind the pressure trough became better organized. This coincided with the rapid initiation of deep convection along the surface cold front. Note also that the phase lag between the pressure and thermal waves has been altered in orientation but not much in distance, as indicated by the axes of the two waves.

In the following 12-h period, the squall line went through its complete life cycle, as we have seen in the previous two subsections. The baroclinic wave structure has also undergone significant changes during this

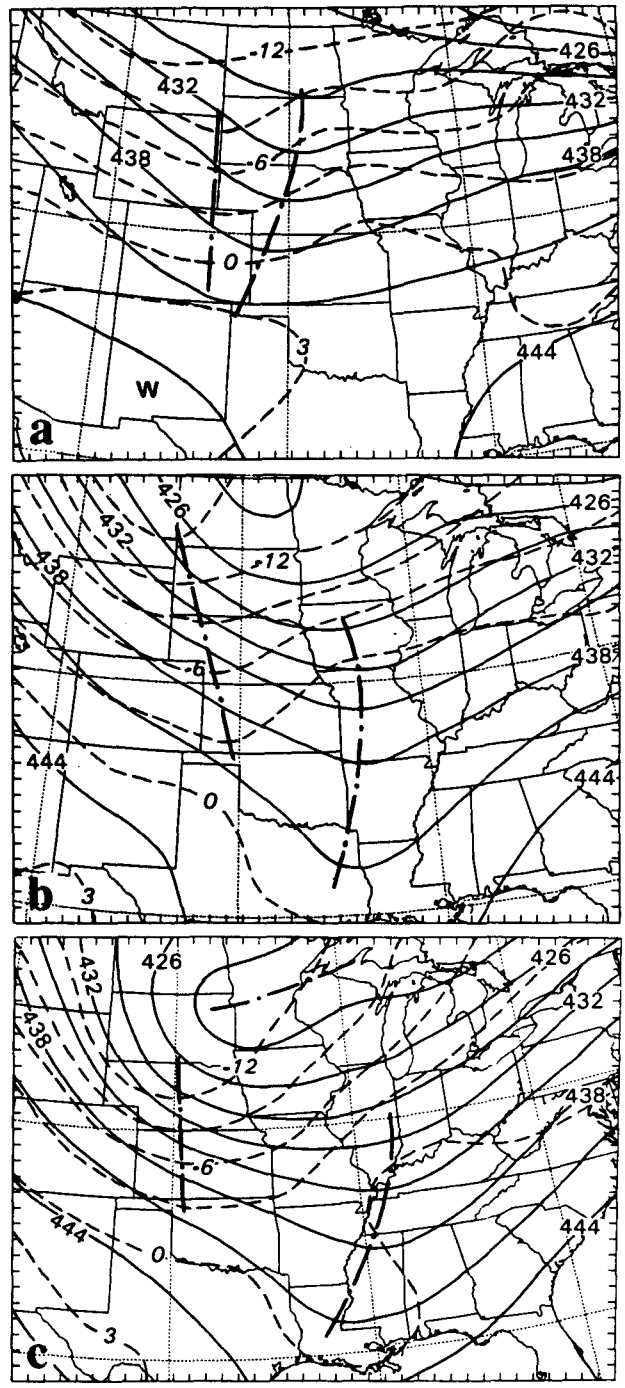

FIG. 12. As in Fig. 2 but for (a) 0000 UTC 11 June, (b) 1200 UTC 11 June, and (c) 0000 UTC 12 June 1985.

period. First, the amplitude of the pressure trough deepened markedly, leading to stronger height gradients along the trough axis (see Fig. 12b). Second, and more importantly, the pressure trough propagated roughly *in pace* with the squall line and was much faster than the midlevel thermal wave. Thus, the different speeds of propagation resulted in an increased *phase lag* between the pressure and thermal waves. According to baroclinic theory, this enhanced phase lag indicates an increased rate of the APE generation and conversion for surface cyclogenesis (see p. 249 in Holton 1992). The result suggests that the interaction of MCSs with baroclinic waves could increase APE in two ways: (a) by releasing latent heat and (b) by producing a more favorable phase lag between the pressure and thermal fields. Previous studies have only considered the first aspect of convective effects on surface cyclogenesis. As the pressure wave deepens, the thermal wave also tends to amplify as a consequence of the enhanced advection, thereby creating a positive feedback between them. Since the thermal trough remained far behind, the squall system appeared to have an indirect impact, through the enhanced larger-scale flow, on the intensification and evolution of the midlevel thermal wave.

At 0000 UTC 12 June, both pressure and thermal troughs have further amplified as they propagated eastward (see Fig. 12c). The midlevel wave amplifications were consistent with the surface baroclinic development since the dissipation of the squall system; hence, it differs from the mechanism that was operative 12 h earlier. The pressure trough axis now extended from eastern Illinois to Mississippi, which was about 450 km to the west of the surface cyclone center. Of importance is that the horizontal extent of the pressure trough has expanded substantially during this 36-h period (cf. Figs. 2 and 12c), as also occurred at the surface. The increase in the trough width appears to differ from the concept described by previous investigators, such as Staley and Gall (1977), Mak (1982), and Emanuel et al. (1987), who showed the enhanced growth rates and shortened wavelengths (or trough widths) as a result of latent heat release within baroclinic disturbances. This difference appears to be attributable to the presence of the convectively enhanced phase lag, which was not considered in the previous studies. A similar scenario seems to have also occurred in the case analyzed by Branick et al. (1988).

Figure 13 shows the same fields as in Fig. 12 but from the corresponding simulations. It is evident that the model reproduces reasonably well the evolution and intensification of the midlevel disturbances. The simulation also provides clearly the evolution of the baroclinic waves as well as the phase lag during the 36-h integration. One can see from the simulations that most of the phase lag is generated in the first 24 h by the squall system, consistent with the surface analyses given in the preceding subsection. At the end of the 36-h simulation, both pressure and thermal waves arrive

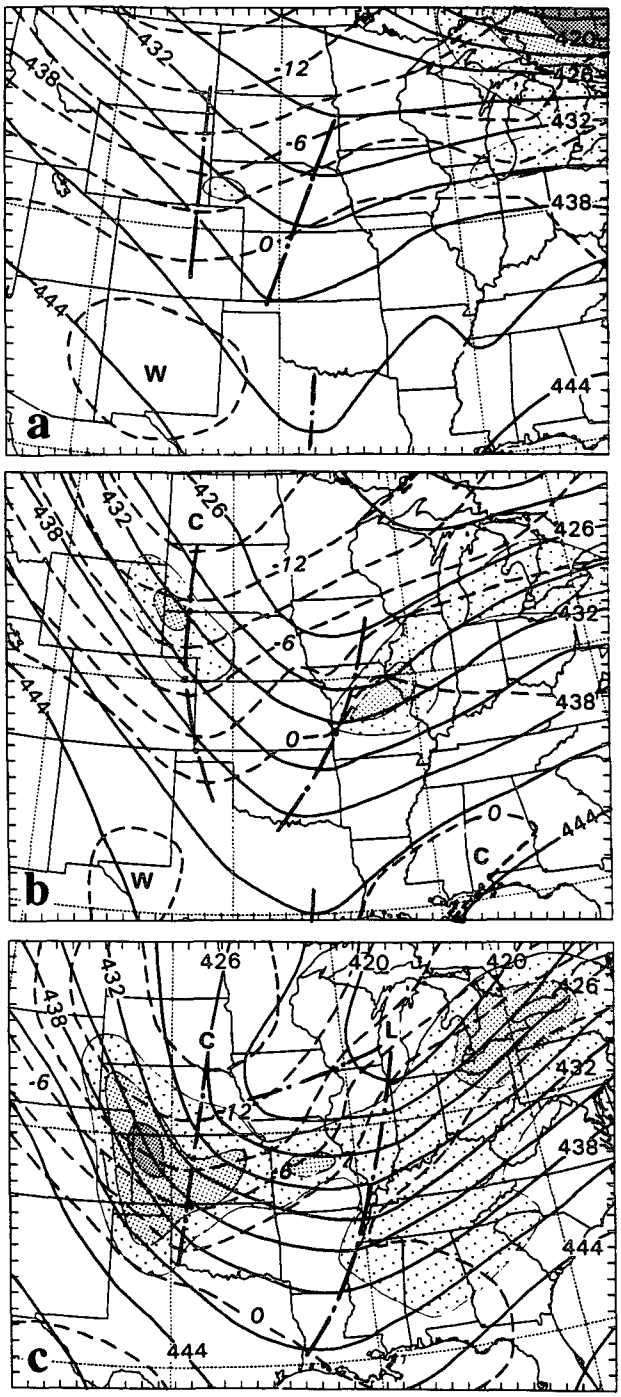

FIG. 13. Distribution of 600-hPa height (solid lines) at intervals of 3 dam and temperature (dashed lines) at intervals of 3°C from (a) 12 h, (b) 24 h, and (c) 36 h simulations valid at 0000 UTC 11 June, 1200 UTC 11 June, and 0000 UTC 12 June 1985. Low-, medium- and high-resolution shadings are used to indicate the distribution of wind speeds greater than 20, 25, and 30 m s^{-1}, respectively. The chained lines indicate the axis of midlevel baroclinic wave troughs.

at positions with intensity and orientation similar to the observed (cf. Figs. 12c and 13c).

After verified against observations, we could use the model simulations to investigate why moist convection tends to produce a pronounced impact on the midlevel pressure but not the thermal waves. Height and temperature maps at upper and lower levels, given in Fig. 14, indicate that the impact has much to do with the structure of convectively generated cooling at low levels and warming aloft. Specifically, the squall system leaves behind a pool of cold air superposed on the low-level baroclinicity (see Figs. 11 and 14b) while producing a warm pocket ahead of the short-wave trough (Fig. 14a); they occur, respectively, in the RTF and FTR branches of the squall circulations (see Figs. 18–20 in ZG). The occurrence of the more marked lower (upper) level cooling (warming) behind (ahead of) the trough axis is as expected for westward-tilted baroclinic waves (e.g., see Figs. 13c and 14). Clearly, such a vertical warming/cooling profile tends to generate hydrostatically midlevel pressure falls on the squall scale, thereby enhancing the midlevel short wave and forcing it to propagate with the system. This analysis is consistent with the observation that the movement of the midlevel short wave coincides with that of the squall's cloud shields. This feature has also been noted in other case studies (e.g., by Zhang and Fritsch 1988a,b). On the other hand, since the convectively generated cold air mass is much less than that associated with the thermal wave and since little net warming/cooling occurs in the midtroposphere, the squall system could not produce any significant effect on the movement of the midlevel thermal wave.

Because of the enhanced phase lag between the pressure and thermal waves, stronger cold advection occurs over a wide region behind the short-wave trough, leading to an increased rate of conversion from APE to kinetic energy (Holton 1992). In agreement with the theory, the tropospheric flow has indeed changed substantially during the 36-h period. For example, the initial wind speeds over the trough region are no more than 15 m s^{-1}; stronger flow is associated with a major low pressure center over northwestern Quebec (see Fig. 2). As the midlevel short wave amplifies, wind speeds increase rapidly with time. The intensity of midlevel flow has more than doubled during the 36-h period—that is, from 15 to >30 m s^{-1} (cf. Figs. 2 and 13c). Meanwhile, the area of the intensified flow expands over the trough region; it occurs more significantly after the dissipation of the squall line (Fig. 13c). This further indicates the more pronounced baroclinic conversion of APE to kinetic energy during this stage, as compared to that which occurred earlier. This phenomenon is also evident in the lower and upper troposphere (Fig. 14), particularly ahead of the pressure trough.

Finally, it should be noted that the NE–SW oriented trough over Iowa (see Fig. 13c) also appears to evolve from the original short wave shown in Fig. 2, although

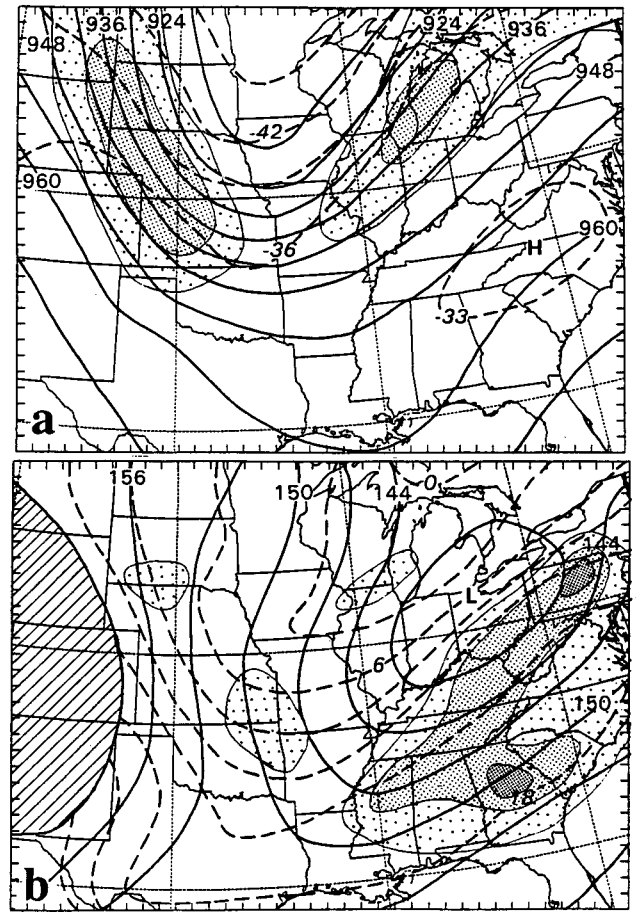

FIG. 14. Distribution of (a) 300-hPa and (b) 850-hPa height (solid: dam) and temperature (dashed: degrees Celsius) from 36-h integration valid at 0000 UTC 12 June 1985. Wind speeds larger than 40 and 50 m s^{-1} at 300 hPa are indicated by respective low- and medium-resolution shadings, whereas at 850 hPa, winds larger than 15, 20, and 25 m s^{-1} are indicated by respective low-, medium-, and high-resolution shadings. The hatched region denotes the intersection of the 850-hPa surface with topography.

it has merged with the major low pressure system to the northeast. This trough does not behave in the same way as the one further downstream because little convective forcing has occurred to the north of the squall system (e.g., see Figs. 6 and 7). It should also be noted that a secondary trough to the south, initially located over New Mexico (Fig. 2), propagates southeastward into the tropical region at a speed slightly faster than the squall-related trough. Since it has a separate vorticity center with different vertical structure (e.g., little westward tilt), this secondary pressure trough does not seem to have an important impact on the propagation of the squall system.

4. Effects of the squall system and large-scale baroclinicity

It is evident from the results presented above that both the squall system and baroclinic processes have

played important but different roles in the surface cyclogenesis. Thus, in this section, we will examine to what extent these two processes contribute to the final spinup of the surface cyclone. This will be done through analyses of the high-resolution model simulations. Specifically, to isolate the effects of large-scale baroclinicity versus the squall system on the surface cyclogenesis, a sensitivity simulation was conducted, in which neither convective nor grid-scale condensation were included (termed the "dry" run),[4] while keeping all the other physical parameters identical to the control (or "moist") simulation. Without the forcing from the diabatic heating, the model atmospheric circulations were dominated only by advective processes. This presumably represents the evolution of the large-scale environment without the influence of the squall line or moist convection in general.

a. Effect of the large-scale baroclinicity

Figure 15 compares the 36-h simulated sea level pressure and 1000–600-hPa thickness from the dry run to the moist run. Of particular relevance here is that in spite of the absence of latent heating, a surface cyclone with a more classic symmetric geometry develops at the end of the 36-h integration. As shown in ZG, there is little evidence of the development of more circular isobars ahead of the surface front, even up to 18 h into the dry simulation (see their Fig. 18). Only a pressure trough is located ahead of the surface cold front, although its central pressure has dropped from 1010 to 1005 hPa during the first 18-h integration. The surface pressure pattern does not become cyclonically organized until after 21 h into the integration, and changes little in intensity thereafter (not shown).

Perhaps such a sequence of the cyclonic development could be expected when considering the interaction of the cold front with high topography (i.e., the Rocky Mountains). Specifically, the initial large-scale baroclinicity and the phase lag between the pressure and thermal waves (Fig. 2), that are more pronounced at 700 hPa (see ZGP), would assist the intensification of the mesolow that is initially located over western Nebraska, if there were no topography. The organized surface cyclone fails to develop in the first 18 hours as the cold front accelerates downslope of the high plateau, because the large-scale baroclinicity is relatively weak compared to the topographical forcing. The Rocky Mountains act as a barrier in forcing the cold current to move southeastward as it subsides anticyclonically from behind the trough axis. The low pressure zone begins to split as the baroclinic system propagates away from the barrier, with the one supported

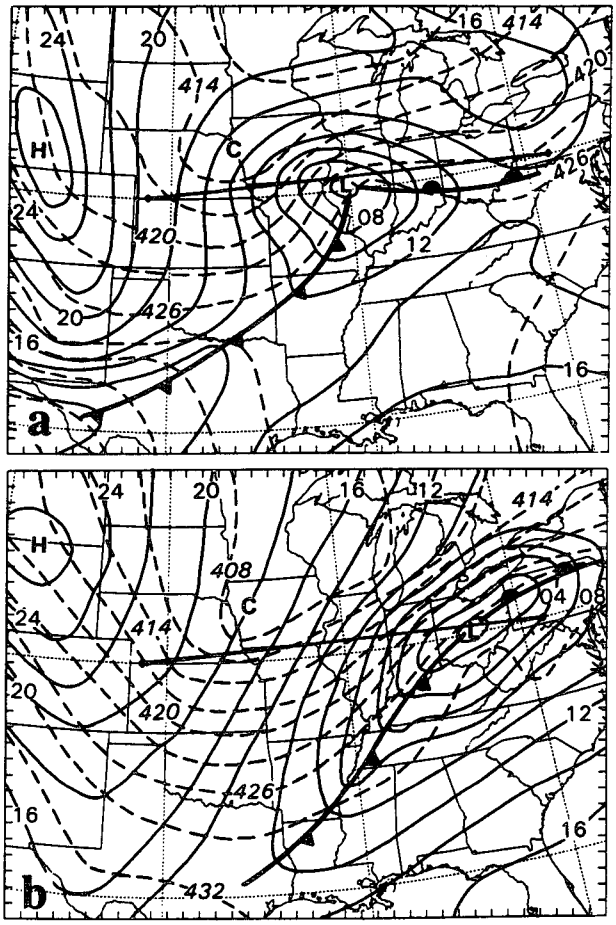

FIG. 15. Distribution of sea level pressure (solid lines) at intervals of 2 hPa and 1000–600 hPa thickness (dashed lines) at intervals of 30 m from (a) 36-h dry simulation, and (b) 36-h control or moist simulation. The west–east oriented line denotes the position of vertical cross sections used in Figs. 17 and 18.

by the midlevel waves moving eastward. These processes appear to account for the tracks of the low-pressure zone in both moist and dry runs, as given in Fig. 1. Then, the subsequent cyclonic developments are dictated more by baroclinic theory. The slight deepening that occurred during the second 18-h period suggests that there may have been some APE conversion to kinetic energy. The juxtaposition of 600-hPa height and temperature fields, given in Fig. 16b, shows that this is indeed the case; much less phase lag or APE is present at the end of the 36-h simulation, as compared to that at the model initial time. Higher up, however, the thermal wave begins to lead the pressure wave (Fig. 16a), as a result of thermal advection in a sheared environment. This negative phase lag implies that both the pressure and thermal waves have amplified to their full extent, and the surface cyclone has begun to fill. It follows that the initial short wave and the cold advection behind it, though weak and shallow, have some positive

[4] Note that the terms, "dry run," "dry cyclone," or "dry dynamics," used herein include the effect of moisture in the virtual temperature computation.

impact on the surface cyclogenesis, and the genesis processes tend to reduce the phase lag between the pressure and thermal waves, as predicted by baroclinic theory.

b. *Effect of moist convection*

The effects of including moist convection on the surface cyclogenesis can be readily examined by comparing the dry and moist runs (i.e., cf. Figs. 15a,b and cf. Figs. 13c, 14, and 16). Several differences can be noticed. First, the moist cyclone moves much faster than the dry cyclone. The difference in position is about 750 km by the end of the 36-h integration. The slower movement in the absence of latent heat release has also been noted by Aubert (1957), Kuo et al. (1991), and others in association with more rapidly deepening surface cyclones. Second, the moist cyclone is 6 hPa deeper, again a common feature that has been found in many of the previous studies (e.g., Anthes and Keyser 1979; Chang et al. 1982; Kuo and Reed 1988). Moreover, the moist cyclone would continue its deepening as a result of increased APE, whereas the dry one has begun to decay owing to the presence of negative phase lag (Fig. 16a). Third, the moist cyclone exhibits much greater horizontal extent along the SW–NE oriented surface cold front, and much stronger and wider troughs with the enhanced phase lag in the low to middle tropospheres, as compared to the "dry" cyclone. This different geometry clearly represents the collective impact of deep convection and stratiform precipitation, that occurred along the dissipated squall line, on the larger-scale cyclonic circulation. As indicated by the NMC analysis, the surface cyclone reached its occlusion 18 hours later with a geometry similar to the dry cyclone (not shown). This evolutionary structure points to the same conclusion that the role of the squall system is to generate additional APE for subsequent surface cyclogenesis through the enhanced horizontal extent and phase lag of the pressure and thermal waves. Once the convectively generated APE is used up, the baroclinic system begins to damp. Fourth, including moist convection increases both the scale and intensity of larger-scale baroclinicity in the lower half portion of the troposphere. As shown in Fig. 15, the 1000–600-hPa thickness gradients between the leading edge of the cold front and the coldest point (i.e., the point "C") are about 210 m (120 m), in the moist (dry) run. The 90 m difference in thickness represents an increase of a 6°C average temperature gradient across that distance in the layer 1000–600 hPa. This is clearly a pronounced contribution of deep convection to the large-scale environment and one of the important factors that could be responsible for the more rapid development of the moist cyclone. In fact, the enhanced baroclinicity results in the development of stronger vertical shears ahead of the short-wave trough (cf. Figs. 13c, 14, and 16a–c); it also produces a much stronger low-level jet

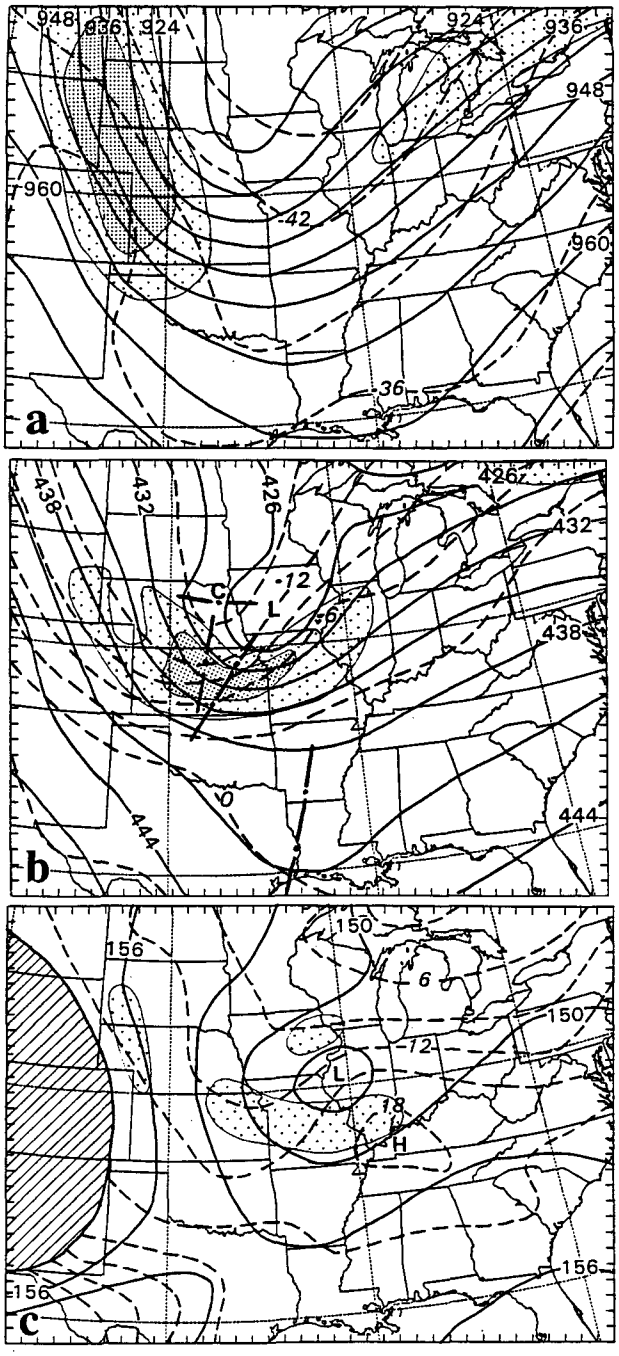

FIG. 16. Distribution of (a) 300-hPa, (b) 600-hPa, and (c) 850-hPa height (solid: dam) and temperature (dashed: degrees Celsius) from 36-h dry integration. Contour intervals and shadings in (a)–(c) are the same as those given in Figs. 13c, 14a, and 14b, respectively.

(e.g., at 850 hPa) ahead of the cold front (e.g., >25 m s^{-1} in the moist run vs <15 m s^{-1} in the dry run).

While the thickness gradients in the moist run are stronger than those in the dry run, the positions of the thickness troughs in these two simulations are very similar at the end of the 36-h integrations; they are oriented

roughly from eastern Nebraska to northern Texas. A similar situation also occurs with the 850-hPa and 600-hPa thermal waves in these two runs (cf. Figs. 13c, 14b, and 16b–c). This implies that *the propagation of the low- to midlevel thermal wave* is primarily governed by *large-scale or adiabatic processes,* in spite of the substantial enhancement of baroclinicity (along the leading edge) by moist convection. This is not surprising because the convectively generated cooling occurs at a scale much smaller and shallower than the thermal wave. The slow displacement of the thermal wave could also be partly attributable to the presence of the Rocky Mountains, which tend to slow the passage of lower-tropospheric cold air masses. On the other hand, ZG showed that the squall system propagates much slower when either the parameterized downdrafts in the Fritsch–Chappell scheme or the grid-scale evaporative cooling was turned off. This reveals that *the propagation of the squall–short wave system* is determined by the interaction between the *convectively generated downdrafts and conditionally unstable conditions in the prestorm environment.* Furthermore, the convectively generated warming in the upper half of the troposphere tends to overcompensate the baroclinically induced cooling ahead of the pressure trough, thus keeping the upper-level baroclinic waves in a favorable phase (cf. Figs. 14a and 16a); otherwise, the low-level baroclinic spinup would be shorter lived.

c. *Interaction between moist convection and its larger-scale environment*

The phase lag described above could also be regarded as a product of the interaction between the squall system and the large-scale environment during the squall's life cycle. Specifically, the squall line is initiated by the baroclinic forcing associated with the cold front and midlevel short wave. Once initiated, however, the subsequent evolution of the squall system is determined by the interaction between the convectively generated circulations and conditionally unstable conditions in the prestorm environment. The baroclinic forcing could only provide a general environment with conditions (e.g., enhanced thermal advection) favorable for convective development but it could not control the evolution of the squall system during this period. Rather, as the squall system intensifies, it influences greatly the baroclinic forcing by enhancing the pressure wave and larger-scale baroclinicity. The squall line decays as it advances into the less conditionally unstable environment to the east of the PRE-STORM network, even though the large-scale baroclinic forcing has significantly intensified. New convective activity ahead of the enhanced cold front does not occur until 1800 UTC June 11 (see Figs. 6 and 7c) when the intensified baroclinic forcing interacts with a conditionally unstable environment that is generated by the development of the daytime boundary layer.

While both latent heat release and the enhanced phase lag produced by deep convection increase the APE of baroclinic systems, they have different impacts on surface cyclogenesis. Specifically, latent heat release, particularly near the center of a cyclone, often occurs in pace with surface cyclogenesis for both baroclinically and convectively driven systems, as reviewed in section 1. In contrast, the development of the increased phase lag implies the presence of a time lag between the intensification of the MCS and subsequent surface cyclogenesis. In the present case, the energy conversion during the squall period is dominated by convectively generated intense circulations, such as the FTR ascending and RTF descending flows, and midlevel mesovortices. Such circulations favor the development of mesohighs and mesolows (see JH and ZG) superposed on the larger-scale surface trough, and the intensification of the midlevel short waves. Thus, the baroclinic spinup of the surface cyclone could not become evident (because it has been obscured by the convective forcing) until after the squall system dissipates and the convectively generated perturbations are absorbed by the larger-scale flow. Of course, when the convectively enhanced phase lag exceeds 90°, deep convection may lead to the weakening of baroclinic systems (Holton 1992). This means that the impact of an MCS on *surface cyclogenesis* may be very sensitive to the particular *location of the MCS within the baroclinic zone.* Nevertheless, the convectively enhanced phase lag in the present case may account for the continued expansion and slow deepening of the large-scale surface trough system during the squall period (see Figs. 4 and 8–11). On the other hand, ZG showed that convectively driven mesocyclogenesis occurs when the latent heating dominates as a result of turning off either the parameterized downdrafts or grid-scale evaporative cooling (see their Figs. 12–16). Because the squall system propagates much more slowly in these circumstances, there is little evidence of the enhancement of the phase lag between the pressure and thermal waves in the midtroposphere.

Although the cyclonic development mechanism after the squall dissipation could be viewed as being similar to that in the dry cyclone (Davis et al. 1993), it should be realized that it is the diabatic heating/cooling associated with the squall system that produces such a baroclinically favorable configuration. Moreover, the large-scale baroclinicity has been substantially enhanced by the development of the MCS. Thus, we may state that even though the baroclinic forcing accounts for the later surface cyclogenesis, it is the squall system that has *conditioned the baroclinic environment for the cyclogenesis* by releasing latent heat and by enhancing the large-scale baroclinicity and the phase lag. Without the moist convection, the surface cyclone in the present case would be weaker, have smaller extent, and dissipate sooner.

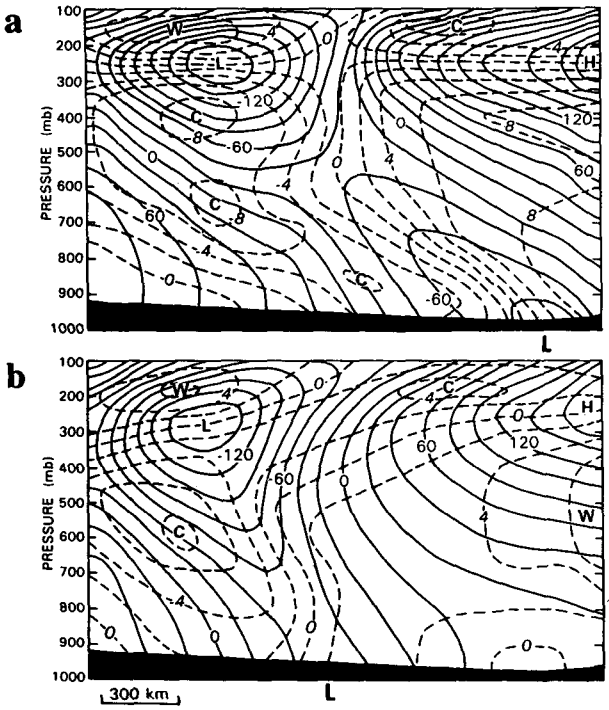

FIG. 17. The west–east vertical cross sections of height deviations (solid lines) at intervals of 20 m and temperature deviations (dashed lines) at intervals of 2°C from (a) 36-h control or moist simulation; and (b) 36-h dry simulation, both taken along the same line given in Fig. 15. The letters, H (L) and W (C), denote the centers of high (low) height and warm (cold) temperature deviations.

d. *Vertical structure of the cyclone*

To further illustrate the relative importance of the squall line and the large-scale baroclinicity in the surface cyclogenesis, Figs. 17a,b show west–east vertical cross sections of height and temperature deviations at the end of the 36-h integration from moist and dry runs, respectively. The cross sections are taken along the same line and roughly through the cyclone centers from these two simulations. All deviations are obtained by deducting their pressure-level averages in the cross section. One can see that the troughs of height deviations in both the moist and dry runs tilt westward with altitude (up to 300 hPa where the large-scale trough is located), and so do the thermal troughs. This type of vertical structure is consistent with the phase lag discussed above and it is again a typical characteristic of baroclinic waves. However, the westward tilt as well as the phase lag between the height and thermal troughs is much greater in the presence of deep convection. The deviation isotherms in the dry case even tilt eastward with height in the lowest layers near the cyclone center. Apparently, these differences are due to the fact that moist convection tends to spread out cold air mass into a wider area in the lower troposphere and helps speed up the movement of the system. The convectively generated thermal gradient is as strong as 14°C/600 km up to 600 hPa. Most of the differences occur ahead of the dry cyclone center as a result of the more rapid displacement by the convective forcing. The moist surface cyclone is now displaced slightly upstream from the upper-level height ridge, whereas the dry surface cyclone is about to be overtaken by the upper-level trough.

To gain insight into the net (direct and indirect) effects of moist convection on its larger-scale environment, Fig. 18a presents the height and temperature differences between the two simulations (i.e., moist minus dry). Because of the different locations of the moist and dry cyclones (Fig. 15), Fig. 18b provides the vertical profiles of height and temperature differences averaged over an area of 2000 km × 600 km. In gen-

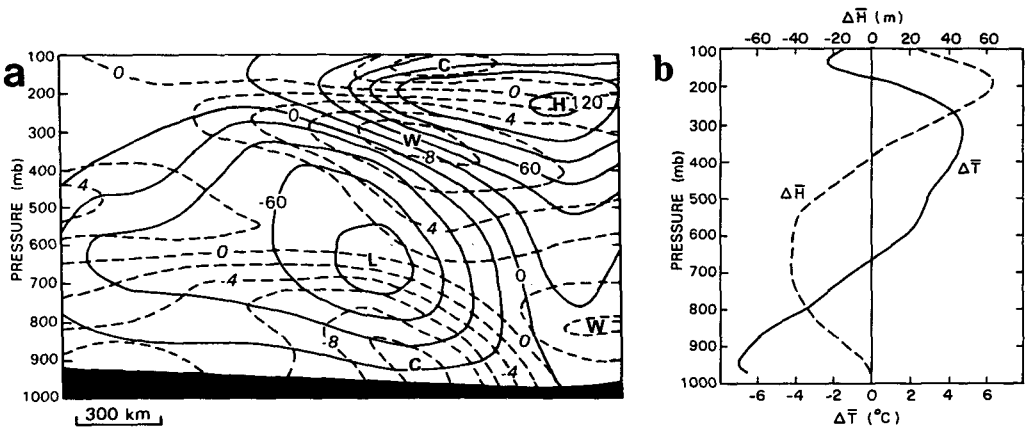

FIG. 18. (a) The west–east vertical cross section of height differences (solid lines) at intervals of 20 m and temperature differences (dashed lines) at intervals of 2°C between the moist and dry runs (i.e., moist minus dry), along the line given in Fig. 15. (b) Area-averaged height (dashed) and temperature (solid) differences between the moist and dry runs, which are taken over a rectangle of 2000 km (i.e., the length of the W–E cross section) by 600 km (symmetric about the cross section). Both are from 36-h integrations.

eral, moist convection produces net warming above the short-wave trough axis with a maximum value of > 8°C occurring near 300 hPa and net cooling below with a minimum value of < -10°C occurring in the lowest layers (Fig. 18a). This convectively generated vertical effect alone is not of particular interest otherwise since one of the roles of moist convection is to stabilize vertically the atmospheric column. However, the collective effects of moist convection result in a deep layer of colder air mass (up to 600 hPa) on a scale of more than 1800 km, revealing again the upscale feedback of the MCS to the large-scale baroclinic environment (cf. Figs. 15b, 17a, and 18a). Of particular relevance here is that such strong warming and cooling over a large scale could account for the amplification of the midlevel short wave and the associated larger-scale flow. The net height difference between the moist and dry runs shows a deficit of more than 80 m near 600 hPa (Fig. 18a). Diabatic heating also produces a net height rise zone throughout the troposphere in the warm sector. The hydrostatic temperature–height relationship is evident from Fig. 18b, which depicts that on average, the moist cyclone experiences pressure falls up to 400 hPa with a greater amplitude occurring in the 750–550 hPa layer. Of particular interest is that in the present case, the height deficit and rise centers are not coherently distributed in the vertical (Fig. 18a). In this sense, one should not treat the convective effects on the surface cyclogenesis as a simple linear addition to the dry dynamics, especially when considering the cumulative influence of moist convection in a sheared environment. Specifically, the net height rise, corresponding to a net warming column up to 200 hPa near the cyclone center, may represent the "barotropic" or direct effect of latent heating that tends to occur in pace with the surface cyclogenesis, just like that associated with tropical cyclogenesis. In contrast, the height deficit associated with the phase lag, maximized at the top leading edge of the cold pool, is more or less dynamically generated as a result of mass evacuation as the colder air subsides (Hirschberg and Fritsch 1991a,b). It would generally take several hours for an MCS to build such a deep layer of cold pool. For example, in the present case the timescale is about 7–9 hours, assuming a propagation speed of 20 m s^{-1} over a 600-km distance from the leading edge of the cool pool at the surface to the location of the midlevel low center. During this period, the large-scale circulation has been substantially altered. Thus, the convectively generated phase lag between the pressure and thermal waves, and the time lag between the intensification of the MCS and the surface cyclogenesis represent the "baroclinic" or indirect contribution of deep convection. Evidently, this nonlinear aspect of MCSs is closely related to the generation of strong *moist downdrafts,* which has been ignored in most of the previous cyclogenesis studies.

e. From a mesolow to a presquall low and a surface cyclone

We have shown how the large-scale environment was initially driven by the weak baroclinicity, and then dominated by convective forcing during the squall period and enhanced baroclinic forcing during the cyclogenesis stage. One may ask how the variations of the large-scale environment affect the evolution of the surface cyclone from a mesolow ahead of the surface cold front at the initial time (Fig. 3) to a presquall mesolow during the squall's period (Fig. 4), and ultimately to the formation of a large-scale surface cyclone (Fig. 11).

As shown in Fig. 3, a closed cyclonic circulation and a 1010-hPa central pressure are initially located over western Nebraska, with a cold front extending southwestward from the low. ZGP showed that during the first 9 hours of the integration, the mesolow travels southeastward to western Kansas (see their Fig. 9 and Fig. 1 herein), where it interacts with a warm front and initiates deep convection. During this presquall period, the mesolow deepens to 1003 hPa. While part of this deepening can be attributed to the model adjustment between the mass and wind fields during the first 5–6 model hours, it is apparent that the cold front and the midlevel short-wave trough support the surface low on its downslope trajectory from the foothills of the Rocky Mountains. Thus, the mesolow is baroclinically driven during this period and accompanied by favorable upward motion over the low. After the initiation of the squall line, the convectively generated compensating subsidence gradually overpowers the baroclinically driven circulation associated with the mesolow (see ZG). Then, the circular-shaped mesolow becomes elongated along and ahead of the leading convective line and gradually resembles the so-called presquall mesolow (see Hoxit et al. 1976); its coverage also increases with time but not its intensity. The elongated presquall low-pressure zone begins to split into two centers after 15 h into the integration, with the one supported by the midlevel trough traveling northeastward (see Fig. 1), as mentioned in section 4a. Near the end of the squall's life cycle, a closed surface low forms to the northeast of the squall system (see Fig. 5).

Now let us examine how the presquall mesolow evolves into the surface cyclone following the dissipation of the squall line. Figures 19a–c show NW–SE cross sections of relative vorticity, superposed by (ground relative) flow vectors along the vertical plane, roughly through the cyclone center from 18, 24, and 30 h simulations. During the dissipation stage (i.e., at 18 h), there are two height trough axes that tilt westward with altitude: one from the surface presquall mesolow (T1) and the other from the wake low or trough (T2). A low- to midlevel mesovortex is located along the convergence zone between the FTR ascending and the RTF descending flows; this vortex is merged from a

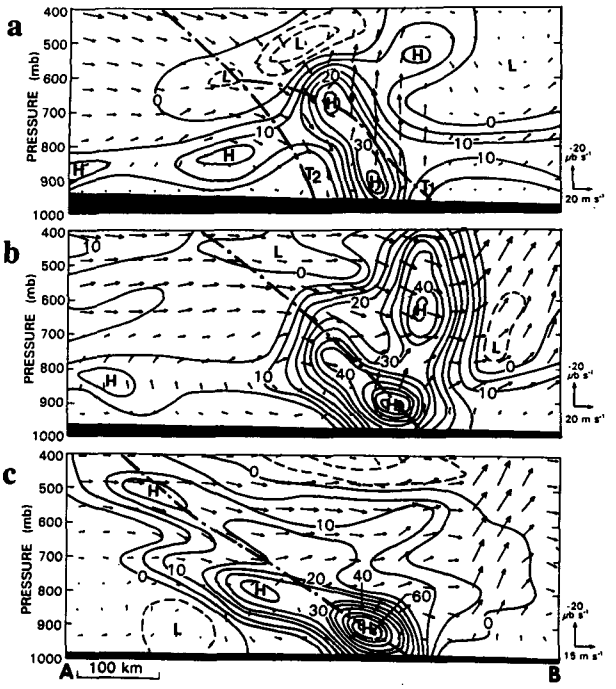

FIG. 19. Vertical cross sections of vertical relative vorticity at intervals of 5×10^{-5} s^{-1} superposed with (ground relative) in-plane flow vectors from (a) 18 h, (b) 24 h, and, (c) 30 h control or moist simulations. Solid (dashed) lines indicate positive (negative) values. They are taken along the lines as given in Figs. 5, 9, and 10, respectively. The chained lines denote the axes of the height deviation troughs (e.g., see Fig. 3 in ZG and Fig. 16 herein) in the cross section. Symbols T1 and T2 represent the troughs associated with the presquall and wake lows, respectively.

leading vortex along the leading convective line and a midlevel wake vortex in the trailing stratiform region (see Zhang 1992). Note that there is little cyclonic vorticity associated with these two surface mesolows. This indicates that the mass field associated with these convectively generated pressure disturbances is still out of balance with the local wind field. In fact, the two surface mesolows are dominated by compensating subsidence, and thus maintained through adiabatic warming during the squall period.

It should be noted that the vorticity structures presented above differ somewhat from those given in Zhang (1992) because of the use of different locations for vertical cross sections. During the squall's decaying stage, some portion of the wake vortex is advected downward and southeastward as colder air subsides anticyclonically in the RTF descending flow, while the rest is advected into the weakening FTR ascending flow. The advection of cyclonic vorticity in the descending flow appears to help enhance the cross-frontal circulations at the lower levels as the surface cyclone intensifies.

At 24 h, when the wake low merges into the presquall low to form the surface cyclone, the main (unbalanced) portion of the midlevel vortex is rapidly advected away in the presence of strong vertical shear. In contrast, the near-surface vortex is pushed forward by the descending cold current, with the center now coinciding with the surface cyclone. Meanwhile, the wind field below 700 hPa gradually adjusts to the mass field, as evidenced by the westward tilt of the vorticity along the height trough. Of importance is a shift of the sign of vertical motion from the subsidence a few hours earlier to relatively strong upward motion at this time near the center of the surface cyclone (cf. Figs. 19a,b). This strong upward motion is consistent with the baroclinic development during this stage.

At 30 h (Fig. 19c), the baroclinic development carries on with the continued spinup of the low-level cyclonic vorticity as a result of intensified vortex stretching. Meanwhile, the surface cyclone accelerates eastward (see Fig. 1), thus reducing the slope of the height trough along which the cyclonic vorticity is distributed. Note the emergence of an upper-level cyclonic vorticity center from the rear, which corresponds closely to the low pressure zone near 300 hPa (cf. Figs. 19c and 17a). At the end of the 36-h integration, the upper- and lower-level cyclonic vorticity centers are roughly aligned along the westwardly tilted trough axis (not shown)—that is, the wind and mass fields are approaching a balanced state. Note also that the flow vectors at this stage exhibit typical circulation characteristics of extratropical cyclones, that is, weak descending flow occurring behind the trough axis, and ascending motion ahead, which is intensified toward the warm sector due to the development of new convection (see Fig. 6).

The results presented above clearly show the relative importance of moist convection versus the large-scale baroclinicity in the surface cyclogenesis from the viewpoint of vorticity. After the dissipation of the squall system, the convectively generated vortices help enhance the low-level cyclonic spinup and intensify the frontal circulation, whereas the mid- to upper-level (unbalanced) portions of mesovortices tend to lose their identity as closed circulations in a baroclinic environment. Thus, only the (gradient) balanced portion of these mesovortices could contribute to the surface cyclogenesis. In the present case, the cyclogenesis occurs as the mesovortex becomes in balance with the low-level pressure trough (or low) that evolves from being convectively driven to baroclinically driven. Without the convective contributions, the baroclinic processes could produce only a weaker, smaller, and shorter-lived surface cyclone.

5. Summary and concluding remarks

In this study, three-dimensional numerical simulations of the 10–12 June 1985 prefrontal squall system were used to investigate the interaction of the MCS with the weak to moderate large-scale baroclinicity in

extratropical cyclogenesis. This work is an extension of the previous 21-h simulation of the same case by ZGP and ZG using the same version of the PSU/NCAR mesoscale model. The model reproduces well the initiation of the squall line, the surface pressure perturbations (e.g., a presquall mesolow, a squall mesohigh, and wake lows), and midlevel circulations during the mature stage, as previously verified against the PRESTORM network data. The prefrontal squall line decays rapidly after 18 h into the integration as it advances into a convectively less unstable environment. During this decaying stage, the model reproduces the merging of the wake low into the presquall low, the formation of the surface cyclone and its subsequent deepening, as well as the amplification of midlevel baroclinic waves. The use of an extended domain in the present study allows us to see that the convectively generated disturbances are embedded within a large-scale cyclonic circulation, which is being enhanced by the convective forcing.

Diagnostic analysis has been performed to examine (i) how the squall system interacts with its larger-scale environment and (ii) how this interaction results in the surface cyclogenesis. It is found that the squall line develops ahead of a weak surface front with the aid of baroclinic forcing. Once initiated, however, the prefrontal squall system is driven by its interaction with the convectively unstable environment ahead. The baroclinic forcing could provide only a favorable environment for the continued generation of convection along the leading line, but it does not control the evolution of the MCS. As the squall system rapidly intensifies and accelerates eastward, it amplifies the midlevel short wave associated with the incipient cyclone and increases the phase lag between the pressure and thermal waves. Meanwhile, the convectively generated downdrafts leave behind an extensive and deep layer of cold air in the cold sector, thereby enhancing the larger-scale baroclinicity in the lower troposphere and the extent of cyclonic circulation. Once the convective forcing weakens, the baroclinic development mechanism takes over, leading to the amplification of the surface cyclone. Our simulation also shows that the balanced portion of the convectively generated mesovortex and low-level pressure trough (or low) produces a positive impact on the subsequent surface cyclogenesis when they are merged into a single entity.

To isolate the effects of moist convection and large-scale baroclinicity on the surface cyclogenesis, a sensitivity simulation is conducted in which all moist convective processes are turned off. By comparing this dry run with the moist run, it is found that in the absence of moist convection the initial large-scale baroclinicity can also produce a surface cyclone, but with much weaker intensity, much smaller horizontal extent, and much slower displacement. The difference fields between the two runs reveal that the midlevel short-wave trough amplifies as a result of the convectively generated cooling below and warming above. Comparisons of the moist run with "no cooling runs" show that the propagation of the squall–short wave system is determined by moist downdrafts interacting with the convectively unstable environment ahead. In contrast, the low to midlevel thermal wave is primarily driven by large-scale adiabatic processes, since the squall-generated cold air mass is still much less than that associated with the thermal wave. As a result of the convective and baroclinic interaction, the phase lag between the midlevel pressure and thermal waves increases as the squall system progresses eastward. Therefore, we may conclude that the roles of the present *squall system* in the *surface cyclogenesis* are not only to *increase the upper-level and decrease the lower-level height of isobaric surfaces,* but also to *enhance the baroclinic environment* by producing a more favorable phase lag between the pressure and thermal waves and by strengthening the existing large-scale baroclinicity. We emphasize, however, that even though the cyclogenesis mechanism after the squall's dissipation is primarily dictated by (enhanced) dry dynamics, it is the diabatic heating/cooling associated with the squall system that produces such baroclinically more favorable conditions for the surface cyclogenesis.

It is important to point out, however, that the above conclusions are only based on a single case analysis. More case studies are needed to generalize our findings. In particular, in the present case, the large-scale baroclinicity and midlevel flow are relatively weak to begin with and the MCS being studied is rather intense; so the convective and baroclinic interactions may be more pronounced than in other summertime situations. Nevertheless, our results underline the importance of accurately predicting the development of MCSs in order to correctly predict certain instances of extratropical cyclogenesis and its associated quantitative precipitation. To achieve this requires the use of high-resolution numerical models with improved initial conditions and appropriate model physics. Failing such attempts, *quantitative precipitation forecasts* could be in serious error, not only for *subsequent mesoscale events,* but also for *larger-scale weather systems* that are well resolved by the model.

Acknowledgments. We would like to thank Lance Bosart, Mike Fritsch, Scott Braum, and an anonymous reviewer for their helpful comments. We benefited from discussions with John Gyakum, Tom Warn, Peter Yau, and Qin Xu. Thanks also go to Ms. U. Seidenfuss for her expert work in the preparation of the figures. The computations were performed at CRAY Y-MP of National Center for Atmospheric Research, which is sponsored by National Science Foundation. The research was supported by Atmospheric Environment Service of Canada and NSF ATM-92-22017.

REFERENCES

Anthes, R. A., 1990: Advances in the understanding and prediction of cyclone development with limited-area fine-mesh models. *Extratropical Cyclones: The Erik Palmén Memorial Volume,* C. W. Newton and E. O. Holopainen, Eds., Amer. Meteor. Soc., 221–253.

——, and D. Keyser, 1979: Tests of a fine-mesh model over Europe and the United States. *Mon. Wea. Rev.,* **107,** 963–984.

——, E.-Y. Hsie, and H. L. Kuo, 1987: Description of the Penn State/NCAR mesoscale model version 4 (MM4). NCAR Tech. Note, NCAR/TN-282, 66 pp.

Aubert, E. F., 1957: On the release of latent heat as a factor in large-scale atmospheric motions. *J. Meteor.,* **14,** 527–542.

Augustine, J. A., and E. J. Zipser, 1987: The use of wind profilers in a mesoscale experiment. *Bull. Amer. Meteor. Soc.,* **68,** 4–17.

Bartels, D. L., and R. A. Maddox, 1991: Midlevel cyclonic vortices generated by mesoscale convective systems. *Mon. Wea. Rev.,* **119,** 104–118.

Biggerstaff, M. I., and R. A. Houze Jr., 1991a: Kinematic and precipitation structure of the 10–11 June 1985 squall line. *Mon. Wea. Rev.,* **119,** 3034–3065.

——, and ——, 1991b: Mid-level vorticity structure of the 10–11 June 1985 squall line. *Mon. Wea. Rev.,* **119,** 3066–3079.

Bosart, L. F., 1981: The Presidents' Day snowstorm of 18–19 February 1979: A sub-synoptic-scale event. *Mon. Wea. Rev.,* **109,** 1542–1566.

——, and F. Sanders, 1981: The Johnstown flood of July 1977: A long-lived convective storm. *J. Atmos. Sci.,* **38,** 1616–1642.

Brandes, E. A., 1990: Evolution and structure of the 6–7 May 1985 mesoscale convective complex and associated vortex. *Mon. Wea. Rev.,* **118,** 109–127.

Branick, M. L., F. Vitale, C.-C. Lai, and L. F. Bosart, 1988: The synoptic and subsynoptic structure of a long-lived severe convective system. *Mon. Wea. Rev.,* **116,** 1335–1370.

Chang, C. B., D. J. Perkey, and C. W. Kreitzberg, 1982: A numerical case study of the effects of latent heating on a developing wave cyclone. *J. Atmos. Sci.,* **39,** 1555–1570.

Charney, J. G., 1947: The dynamics of long waves in a baroclinic westerly current. *J. Meteor.,* **4,** 135–163.

——, and A. Eliassen, 1964: On the growth of the hurricane depression. *J. Atmos. Sci.,* **21,** 68–75.

Cunning, J. B., 1986: The Oklahoma–Kansas preliminary regional experiment for STORM-Central. *Bull. Amer. Meteor. Soc.,* **67,** 1478–1486.

Danard, M. B., 1964: On the influence of released latent heat on cyclone development. *J. Appl. Meteor.,* **3,** 27–37.

——, 1966: On the contribution of released latent heat to changes in available potential energy. *J. Appl. Meteor.,* **5,** 81–84.

Davis, C. A., and K. A. Emanuel, 1991: Potential vorticity diagnosis of cyclogenesis. *Mon. Wea. Rev.,* **119,** 1929–1953.

——, M. T. Stoelinga, and Y.-H. Kuo, 1993: The integrated effect of condensation in numerical simulations of extratropical cyclogenesis. *Mon. Wea. Rev.,* **121,** 2309–2330.

Dudhia, J., 1989: Numerical study of convection observed during the winter monsoon experiment using a mesoscale two-dimensional model. *J. Atmos. Sci.,* **46,** 3077–3107.

Eady, E. T., 1949: Long waves and cyclone waves. *Tellus,* **1,** 33–52.

Emanuel, A., M. Fantini, and A. J. Thorpe, 1987: Baroclinic instability in an environment of small stability to slantwise moist convection. Part I: Two-dimensional model. *J. Atmos. Sci.,* **44,** 1559–1573.

Fritsch, J. M., and C. F. Chappell, 1980: Numerical prediction of convectively driven mesoscale pressure systems. Part I: Convective parameterization. *J. Atmos. Sci.,* **37,** 1722–1733.

——, J. D. Murphy, and J. S. Kain, 1994: Warm-core vortex amplification over land. *J. Atmos. Sci.,* **51,** 1780–1807.

Gallus, W. A., Jr., and R. H. Johnson, 1991: Heat and moisture budgets of an intense midlatitude squall line. *J. Atmos. Sci.,* **48,** 122–146.

Gyakum, J. R., 1983: On the evolution of the *QE II* storm. Part II: Dynamic and thermodynamic structure. *Mon. Wea. Rev.,* **111,** 1156–1173.

Hirschberg, P. A., and J. M. Fritsch, 1991a: Tropopause undulations and the development of extratropical cyclones. Part I: Overview and observations from a cyclone event. *Mon. Wea. Rev.,* **119,** 496–517.

——, and ——, 1991b: Tropopause undulations and the development of extratropical cyclones. Part II: Diagnostic analysis and conceptual model. *Mon. Wea. Rev.,* **119,** 518–550.

Holton, J. R., 1992: *An Introduction to Dynamic Meteorology.* Academic Press, 511 pp.

Hoskins, B. J., 1990: Theory of extratropical cyclones. *Extratropical Cyclones: The Erik Palmén Memorial Volume,* C. W. Newton and E. O. Holopainen, Eds., Amer. Meteor. Soc., 64–80.

——, M. E. McIntyre, and A. W. Robertson, 1985: On the use and significance of isentropic potential vorticity maps. *Quart. J. Roy. Meteor. Soc.,* **111,** 877–946.

Houze, R. A., Jr., 1977: Structure and dynamics of a tropical squall line system. *Mon. Wea. Rev.,* **105,** 1540–1567.

——, S. A. Rutledge, M. I. Biggerstaff, and B. F. Smull, 1989: Interpretation of Doppler weather-radar displays of midlatitude mesoscale convective systems. *Bull. Amer. Meteor. Soc.,* **70,** 608–619.

Hoxit, L. R., C. F. Chappell, and J. M. Fritsch, 1976: Formation of mesolows or pressure troughs in advance of cumulonimbus clouds. *Mon. Wea. Rev.,* **104,** 1419–1428.

Hsie, E.-Y., R. A. Anthes, and D. Keyser, 1984: Numerical simulation of frontogenesis in a moist atmosphere. *J. Atmos. Sci.,* **41,** 2581–2594.

Johnson, R. H., 1976: The role of convective-scale precipitation downdrafts in cumulus and synoptic-scale interactions. *J. Atmos. Sci.,* **33,** 1890–1910.

——, and P. J. Hamilton, 1988: The relationship of surface pressure features to the precipitation and airflow structure of an intense midlatitude squall line. *Mon. Wea. Rev.,* **116,** 1444–1471.

——, and D. L. Bartels, 1992: Circulations associated with a mature-to-decaying midlatitude mesoscale convective system. Part II: Upper-level features. *Mon. Wea. Rev.,* **120,** 1301–1320.

Kuo, H. L., 1965: On formation and intensification of tropical cyclones through latent heat release by cumulus convection. *J. Atmos. Sci.,* **22,** 40–63.

Kuo, Y.-H., and R. J. Reed, 1988: Numerical simulation of an explosively deepening cyclone in the eastern Pacific. *Mon. Wea. Rev.,* **116,** 2081–2105.

——, M. A. Shapiro, and E. G. Donall, 1991: The interaction between baroclinic and diabatic processes in a numerical simulation of a rapidly intensifying extratropical marine cyclone. *Mon. Wea. Rev.,* **119,** 368–384.

Mak, M., 1982: On moist quasi-geostrophic baroclinic instability. *J. Atmos. Sci.,* **39,** 2028–2037.

Margules, M., 1903: Über die Energie der Stürme. Jahr. kaisk. Zentrum für Meteorologie, Vienna. [English translation by C. Abbel, 1910, *Smithsonian Misc. Coll.,* **51,** 533–595.]

Menard, R. D., and J. M. Fritsch, 1989: A mesoscale convective complex-generated inertially stable warm core vortex. *Mon. Wea. Rev.,* **117,** 1237–1261.

Pauley, P. M., and P. J. Smith, 1988: Direct and indirect effects of latent heat release on a synoptic-scale wave system. *Mon. Wea. Rev.,* **116,** 1209–1235.

Reed, R. J., 1990: Advances in knowledge and understanding of extratropical cyclones during the past quarter century: An overview. *Extratropical Cyclones: The Erik Palmén Memorial Volume,* C. W. Newton and E. O. Holopainen, Eds., Amer. Meteor. Soc., 27–45.

Riehl, H., and J. S. Malkus, 1961: Some aspects of hurricane Daisy, 1958. *Tellus,* **13,** 181–213.

Rutledge, S. A., R. A. Houze Jr., M. I. Biggerstaff, and T. Matejka, 1988: The Oklahoma–Kansas mesoscale convective system of 10–11 June 1985: Precipitation structure and single-Doppler radar analysis. *Mon. Wea. Rev.,* **116,** 1409–1430.

Sanders, F., and J. R. Gyakum, 1980: Synoptic–dynamic climatology of the "bomb." *Mon. Wea. Rev.*, **108,** 1589–1606.

Smith, P. J., P. M. Dare, and S.-J. Lin, 1984: The impact of latent heat release on synoptic-scale vertical motions and the development of an extratropical cyclone system. *Mon. Wea. Rev.*, **112,** 2421–2430.

Smull, B. F., and R. A. Houze Jr., 1987: Rear inflow in squall lines with trailing stratiform precipitation. *Mon. Wea. Rev.*, **115,** 2869–2889.

Staley, D. O., and R. L. Gall, 1977: On the wavelength of maximum baroclinic instability. *J. Atmos. Sci.*, **34,** 1679–1688.

Tracton, M. S., 1973: The role of cumulus convection in the development of extratropical cyclones. *Mon. Wea. Rev.*, **101,** 573–593.

Uccellini, L. W., 1990: Processes contributing to the rapid development of extratropical cyclones. *Extratropical Cyclones: The Erik Palmén Memorial Volume,* C. W. Newton and E. O. Holopainen, Eds., Amer. Meteor. Soc., 81–105.

——, R. A. Pettersen, K. F. Brill, P. J. Kocin, and J. J. Tuccillo, 1987: Synergistic interactions between an upper-level jet steak and diabatic processes that influence the development of a low-level jet and a secondary coastal cyclone. *Mon. Wea. Rev.*, **115,** 2227–2261.

Zhang, D. L., 1989: The effect of parameterized ice microphysics on the simulation of vortex circulation with a mesoscale hydrostatic model. *Tellus,* **41A,** 132–147.

——, 1992: The formation of cooling-induced mesovortex in the trailing stratiform region of a midlatitude squall line. *Mon. Wea. Rev.*, **120,** 2763–2785.

——, and R. A. Anthes, 1982: A high-resolution model of the planetary boundary layer—sensitivity tests and comparison with SESAME-79 data. *J. Appl. Meteor.*, **21,** 1594–1609.

——, and J. M. Fritsch, 1987: Numerical simulation of the meso-β scale structure and evolution of the 1977 Johnstown flood. Part II: Inertially stable warm-core vortex and the mesoscale convective complex. *J. Atmos. Sci.*, **44,** 2593–2612.

——, and ——, 1988a: Numerical sensitivity experiments of varying model physics on the structure, evolution and dynamics of two mesoscale convective systems. *J. Atmos. Sci.*, **45,** 261–293.

——, and ——, 1988b: A numerical investigation of a convectively generated, inertially stable, extratropical warm-core mesovortex over land. Part I: Structure and evolution. *Mon. Wea. Rev.*, **116,** 2660–2687.

——, and K. Gao, 1989: Numerical simulation of an intense squall line during 10–11 June 1985 PRE-STORM. Part II: Rear inflow, surface pressure perturbations and stratiform precipitation. *Mon. Wea. Rev.*, **117,** 2067–2094.

——, H.-R. Chang, N. L. Seaman, T. T. Warner, and J. M. Fritsch, 1986: A two-way interactive nesting procedure with variable terrain resolution. *Mon. Wea. Rev.*, **114,** 1330–1339.

——, K. Gao, and D. B. Parsons, 1989: Numerical simulation of an intense squall line during 10–11 June 1985 PRE-STORM. Part I: Model verification. *Mon. Wea. Rev.*, **117,** 960–994.

——, J. S. Kain, J. M. Fritsch, and K. Gao, 1994: Comments on "Parameterization of convective precipitation in mesoscale numerical models: A critical review." *Mon. Wea. Rev.*, **122,** 2222–2231.

Zipser, E. J., 1977: Mesoscale and convective-scale downdrafts as distinct components of squall line structure. *Mon. Wea. Rev.*, **105,** 1568–1589.